UNIVERSITY OF CALIFORNIA SAN DIEGO

Developmental Immaturity of Siglec Receptor Expression on Neonatal Alveolar Macrophages Predisposes to Severe Group B Streptococcal Infection

A Dissertation Submitted in Partial Satisfaction of the Requirements for the Degree

Doctor of Philosophy

in

Biomedical Sciences

by

Sean Joseph Lund

Committee in charge:

Professor Lawrence Prince, Chair
Professor Christopher Glass
Professor Stephen Hedrick
Professor Victor Nizet
Professor Xin Sun

2020

The Dissertation of Sean Joseph Lund is approved and it is acceptable in quality and form for publication on microfilm and electronically:

Chair

University of California San Diego

2020

DEDICATION

I would like to dedicate this dissertation to my Mom and Dad for their unwavering and total support. I could not have accomplished what I have been able to without them.

TABLE OF CONTENTS

Signature Page iii

Dedication iv

Table of Contents v

List of Abbreviations vi

List of Symbols ix

List of Figures and Tables x

Acknowledgements xii

Vita xiv

Abstract of the Dissertation xvi

Introduction 1

Materials and Methods 11

Results 18

Discussion 34

Appendix: Figures and Tables 40

References 71

LIST OF ABBREVIATIONS

α2−3 – alpha anomer of sialic acid linked from 2nd carbon to 3rd carbon of galactose

α2−6 – alpha anomer of sialic acid linked from 2nd carbon to 6th carbon of galactose

ΔcpsD – GBS capsule mutant

ΔneuA – GBS sialic acid mutant

μL – microliter

Ad – Adult

AIMϕ – Alveolar Interstitial Macrophage

AMϕ – Alveolar Macrophage

APC – Allophycocyanin

ATAC-seq – Assay for Transposase-Accessible Chromatin using sequencing

BAL – Bronchoalveolar Lavage

BIMϕ – Bronchial Interstitial Macrophage

BV421 – Brilliant Violet 421

CD – Cluster of Differentiation

CFU – Colony-forming unit

ChIP-seq – Chromatin Immunoprecipitation Sequencing

Csf2 – GM-CSF, Granulocyte-Macrophage Colony Stimulating Factor

Csf2$^{-/-}$ – GM-CSF, Granulocyte-Macrophage Colony Stimulating Factor KO mice

CXCL1 – C-X-C Motif Ligand 1

Cy7 – Cyanine 7

d - days

DC – Dendritic Cell

EMPs – Erythromyeloid Precursors

FACS – Fluorescence-Activated Cell Sorting

GBS – Group B *Streptococcus* (*Streptococcus agalactiae*)

h – hours

HSCs – Hematopoietic Stem Cells

IFN-α – Interferon alpha

IFN-γ – Interferon gamma

FI – Fluorescent Intensity

FITC – Flourescein Isothiocyanate

IF – Immunofluorescence

IL-1β – Interleukin 1β

IL-6 – Interleukin 6

IMϕ – Interstitial Macrophage

Juv – Juvenile

KO - Knockout

LPS – lipopolysaccharide

min – minute

mL – milliliter

MPs – Myeloid Precursors

NAMϕ – Nerve and Airway Associated Macrophage

Neo - Neonate

PCR – Polymerase Chain Reaction

PerCP – Peridinin Chlorophyll

PE – Phycoerythrin

PMN – Polymorphonuclear Cell

Pre-AMϕ – Pre-alveolar macrophage

qPCR – Quantitative Polymerase Chain Reaction

RG – rosiglitazone

SEM – Standard Error of the Mean

Sia – Sialic Acid

Sig-E – Siglec-E

Sig-$E^{-/-}$ – Siglec-E KO mice

Sig-F – Siglec-F

Siglec – Sialic acid-binding immunoglobulin-like lectin

Sn – Sialoadhesin

STAT – Signal Transducer and Activator of Transcription

TFBS – Transcription Factor Binding Site

THP – Tamm-Horsfall Protein / Uromodulin

$THP^{-/-}$ – Tamm-Horsfall Protein / Uromodulin KO mice

TNF-α – Tumor Necrosis Factor α

TSS – Transcription Start Site

UTR – Untranslated Region

WT – Wild Type

LIST OF SYMBOLS

-/- – Homozygous genetic knockout

± – Plus or Minus

α2−3 – alpha anomer of sialic acid linked from 2nd carbon to 3rd carbon of galactose

α2−6 – alpha anomer of sialic acid linked from 2nd carbon to 6th carbon of galactose

Δ – Bacterial mutant

ϕ – Macrophage

$(CD11b)^{hi}$ – High expression of CD11b as measured by flow cytometry

$(CD11b)^{int}$ – Intermediate expression of CD11b as measured by flow cytometry

$(CD11b)^{lo}$ – Low expression of CD11b as measured by flow cytometry

$(CD11b)^{+}$ – Positive expression of CD11b as measured by flow cytometry

$(CD11b)^{-}$ – Negative expression of CD11b as measured by flow cytometry

Cxcl1 – Mouse gene name of CXCL1

Il1b – Mouse gene name of IL-1β

Il6 – Mouse gene name of IL-6

SIGLEC1 – Human gene name of Siglec-1

SIGLEC9 – Human gene name of Siglec-9, paralog of mouse Siglec-E

Siglec1 – Mouse gene name of Sn

Siglece – Mouse gene name of Siglec-E

LIST OF FIGURES AND TABLES

Figure 1: Increased Mortality and Persistence of Lung Injury in Neonatal GBS Infection 40

Figure 2: Delayed Kinetics of Lung Inflammation and GBS Clearance by Alveolar Macrophages in Neonatal GBS Pneumonia 42

Figure 3: Mature AMϕs are Required for Rapid GBS Clearance 44

Figure 4: Developmental Maturation of Lung Myeloid Siglec Expression 46

Figure 5: Developmental Immaturity of AMϕ Siglec-Sialic Acid Detection Contributes to Neonatal GBS Susceptibility 48

Figure 6: Sn Expression Declines Over Time Following GBS Infection 51

Figure 7: The Sia-Siglec-E Interaction Mediates Decreased Sn Expression Following Infection 53

Figure 8: *Siglec1* is Regulated by the STAT Pathway and is Differentially Accessible in the Adult 55

Figure 9. RG, IFN-α,γ Did Not Increase Sn Expression on the First Day of Life 57

Figure 10: Sialic Acid is Not Expressed in the Developing Fetal Lung 59

Figure 11: Loss of THP Alters Neonatal Siglec-E and Siglec-F Receptor Expression 61

Figure S1: Gating Strategy for Measuring Siglec Receptor Expression on Lung Macrophage Populations. 63

Figure S2: Changes in Macrophage Marker Expression Following GBS Infection 65

Figure S3: Effects of Clodronate on Sn Expression and Backgating Analysis 67

Table 1: qPCR Primers 69

Table 2: Immune Cell Population Definitions 70

ACKNOWLEDGEMENTS

This dissertation contains material as it appears in "Developmental Immaturity of Siglec Receptor Expression on Neonatal Alveolar Macrophages Predisposes to Severe Group B Streptococcal Infection" published in *iScience*. The dissertation author was the primary investigator and author of this paper,

> Lund, S. J., Patras, K.A., Kimmey, J.M., Yamamura, A., Butcher, L.D., Del Rosario, P.G.B., Hernandez, G.E., McCoy, A.M., Lakhdari, O., Nizet, V., Prince, L.S. (2020). Developmental Immaturity of Siglec Receptor Expression on Neonatal Alveolar Macrophages Predisposes to Severe Group B Streptococcal Infection. *iScience*, p.101207.

Other material in this dissertation has been adapted from the below manuscript currently in preparation for submission.

> Lund, S. J., Del Rosario, P.G.B., Yamamura, A., Patras, K.A., Butcher, L.D., Lakhdari, O., Nizet, V., Prince, L.S. Sialic Acid-Siglec-E Interactions Regulate Expression of Sialoadhesin and Alveolar Macrophage Development.

I would like to acknowledge Drs. Kathryn Patras, Jacqueline Kimmey, and Victor Nizet for kindly providing the strains of GBS and the Sig-E$^{-/-}$ mice. Their expertise helped make this dissertation possible.

I would like to acknowledge Asami Yamamura, and Drs. Lindsay Butcher, Omar Lakhdari, Alyssa McCoy, and Lawrence Prince for their assistance in lung pathology scoring in Figure 1.

I would like to acknowledge Dr. Pamela Del Rosario for kindly providing the data used in Figure 6.

I would like to acknowledge Asami Yamamura for kindly providing the ATAC-seq data used in Figure 8.

I would like to acknowledge Dr. Kathryn Patras for kindly providing the THP ELISA data in Figure 11.

I would like to acknowledge the UCSD Moores Cancer Center Tissue Technology Shared Resource for their assistance in slide preparation and histology staining. I also would like to acknowledge the UCSD Microscopy Core for the use of their Leica SP5 Confocal Microscope.

This work was supported by NIH grants HL146066 (S.J.L.), AI142864 (L.S.P. and V.N.), HL126703 (L.S.P.), and P01-HL107150 (V.N.). The UCSD Microscopy is supported by NIH grant NS047101, and the UCSD Tissue Technology Shared Resource is supported by an NCI Cancer Center Support Grant (CCSG Grant P30CA23100).

VITA

2013 Bachelor of Science, University of California San Diego

2014 Master of Science, University of California San Diego

2020 Doctor of Philosophy, University of California San Diego

PUBLICATIONS

1. Lund, S. J., Patras, K.A., Kimmey, J.M., Yamamura, A., Butcher, L.D., Del Rosario, P.G.B., Hernandez, G.E., McCoy, A.M., Lakhdari, O., Nizet, V., Prince, L.S. (2020). Developmental Immaturity of Siglec Receptor Expression on Neonatal Alveolar Macrophages Predisposes to Severe Group B Streptococcal Infection. iScience, p.101207.

2. Lakhdari, O., Yamamura, A., Hernandez, G.E., Anderson, K.K., Lund, S. J., Oppong-Nonterah, G.O., Hoffman, H.M. and Prince, L.S. (2019). Differential Immune Activation in Fetal Macrophage Populations. Scientific Reports, 9(1), p.7677.

3. Henningham A., Davies M. R., Uchiyama S., van Sorge N. M., Lund S., Chen K. T., Walker M. J., Cole J. N., Nizet V. (2018). Virulence role of the GlcNAc side chain of the Lancefield cell wall carbohydrate antigen in non-M1-serotype group A Streptococcus. mBio 9:e02294-17.

4. Lund, S. J., Portillo, A., Cavagnero, K., Baum, R. E., Naji, L. H., Badrani, J. H., Mehta, A., Croft, M., Broide, D. H., and Doherty, T. A. (2017). Leukotriene C4 Potentiates IL-33–Induced Group 2 Innate Lymphoid Cell Activation and Lung Inflammation. Journal of Immunology. 199 (3), 1096-1104.

5. Banerjee, I., Carrion, K., Serrano, R., Dyo, J., Sasik, R., Lund, S., ... & Nigam, V. (2015). Cyclic stretch of embryonic cardiomyocytes increases proliferation, growth, and expression while repressing TGF-β signaling. Journal of molecular and cellular cardiology, 79, 133-144.

6. Walford, H. H., Lund, S. J., Baum, R. E., White, A. A., Bergeron, C. M., Husseman, J. … & Doherty, T. A. (2014). Increased ILC2s in the eosinophilic nasal polyp endotype are associated with corticosteroid responsiveness. Clin. Immunol. 155 (1), 126-135.

7. Scott, D. R., Doherty, T. A., Khorram, N., Lund, S., Baum, R., Chang, J., ... & Broide, D. H. (2014). Allergen Challenge Increases Peripheral Blood CD84+ ILC2 In Allergic Rhinitis. Journal of Allergy and Clinical Immunology, 133(2), AB237.

8. Lund, S., Walford, H. H., & Doherty, T. A. (2013). Type 2 Innate Lymphoid Cells in Allergic Disease. Current Immunology Reviews. 9 (4), 214-221.

9. Kim, H. K., Lund, S., Baum, R., Khorram, N., Rosenthal, P., & Doherty, T. (2013). Innate Type-2 Response to Alternaria Extract Enhances Ryegrass-induced Lung inflammation. International Archives of Allergy and Immunology. 163(2):92-105.

10. Kim, H. K., Baum, R., Lund, S., Khorram, N., Yang, S. L., Chung, K. R., & Doherty, T. A. (2013). Impaired induction of allergic lung inflammation by Alternaria alternata mutant MAPK homologue Fus3. Exp Lung Res. 39(9):399-409.

11. Doherty, T. A., Khorram, N., Lund, S., Mehta, A. K., Croft, M., & Broide, D. H. (2013). Lung type 2 innate lymphoid cells express cysteinyl leukotriene receptor 1, which regulates TH 2 cytokine production. Journal of Allergy and Clinical Immunology. 132 (1), 205-213.

FIELDS OF STUDY

Major Field: Immunology

Studies in Asthma and Allergy
Professor Taylor Doherty

Studies in Neonatology and Immune Development
Professor Lawrence Prince

Major Field: Infectious Disease

Studies in Bacteriology
Professor Victor Nizet

ABSTRACT OF THE DISSERTATION

Developmental Immaturity of Siglec Receptor Expression on Neonatal Alveolar Macrophages Predisposes to Severe Group B Streptococcal Infection

by

Sean Joseph Lund

Doctor of Philosophy in Biomedical Sciences

University of California San Diego, 2020

Professor Lawrence Prince, Chair

Streptococcus agalactiae (Group B *Streptococcus*, GBS) is the most common neonatal pathogen capable of causing devastating disease in newborns, yet healthy adults are largely unaffected. The cellular and molecular mechanisms for neonatal susceptibility to GBS pneumonia and sepsis are incompletely understood. Here we optimized a mouse model of GBS pneumonia to test the role of alveolar macrophage (AMϕ) maturation in host vulnerability to severe disease. Compared with juvenile and adult mice, neonatal mice

infected with GBS had increased mortality and persistence of lung injury. In addition, neonatal mice were defective in GBS phagocytosis and killing. AMϕ depletion and disruption of AMϕ differentiation in $Csf2^{-/-}$ mice both impaired GBS clearance. AMϕ engage the heavily sialylated GBS capsule via the cell surface Siglec receptors Sialoadhesin (Sn) and Siglec-E. Newborn AMϕ expressed significantly lower levels of Sn, although both newborn and adult AMϕ expressed Siglec-E. Sn is exclusively expressed by $CD11b^{lo}$ and $CD11b^{hi}$ AMϕ, while Siglec-E is more commonly expressed by lung myeloid cells. AMϕ Sn expression decreased after GBS infection in both adults and neonates, this decrease seemed to be mediated by the GBS Sia-Siglec-E ligation. The GBS Sia mutant, ΔneuA, failed to decrease Sn expression in either adults or neonates. Cell surface protein expression of Sn also decreased at 24 h after GBS infection in the WT neonates, however, $Sig\text{-}E^{-/-}$ neonates maintained surface expression of Sn at 24 h of infection. We propose that a developmental delay in Sn expression on AMϕ may prevent effective killing and clearing of GBS from the newborn lung. Next we investigated the impact host Sia could have on AMϕ development and responsiveness to infection. While the fetal lung lacks expression of α2-3 Sia in the lung, the major sialylated glycoprotein in the urine, Tamm-Horsfall Protein (THP), was found in the fetal lung. $THP^{-/-}$ neonates, at PND1, 2, and 8 all showed decreased expression of Siglec-E, and higher expression of Siglec-F at PND2. We hypothesize that the developing fetus aspirates amniotic fluid, of which a major component is fetal urine containing THP, into the lung during gestation bringing a source of Sia into the lungs and regulates fetal AMϕ development and suppresses inflammatory activity.

INTRODUCTION

Streptococcus agalactiae (group B *Streptococcus*, GBS) remains a potentially devastating neonatal pathogen. Globally, GBS colonizes the vaginal or rectal epithelium of an estimated 21.7 million pregnant women (1). The leading infectious cause of neonatal mortality, GBS, is estimated to cause 150,000 newborn deaths worldwide each year (2, 3). Infants are exposed to GBS during passage through the birth canal or via ascending infection through the amniotic membranes. GBS neonatal disease is commonly classified as early-onset disease (<7 days of age) or late-onset disease (7 days–6 months of age) (4-7). In the majority of cases of early-onset disease, newborns aspirate contaminated amniotic or vaginal fluid, developing clinical signs of pneumonia, lung injury, and sepsis within the first few hours of life. In contrast, late-onset GBS infections tend to present days later with bacteremia and a high risk of meningitis (8). Serious GBS infections in otherwise healthy older children and adults are rare, although non-pulmonary invasive disease is increasingly reported in individuals with lowered immunity such as the elderly, pregnant women, and those with diabetes or cancer (9, 10).

GBS is an encapsulated gram-positive bacterium possessing a few key virulence factors involved in the pathogenesis of infections. Tissue damage in GBS infections is largely caused by the pore-forming toxins, β-hemolysin and cytolysin. The production of β-hemolysin and cytolysin enables invasion into the capillaries by breakdown of structural components and loss of barrier integrity (11). The effects of β-hemolysin and cytolysin can be limited or blocked by surfactant, most notably by dipalmitoyl phosphatidylcholine (11, 12), a major phospholipid in surfactant. The developing fetus begins to produce surfactant and continues into the neonatal period. Less surfactant, and thus less dipalmitoyl

phosphatidylcholine, in the lung could render newborns more susceptible to the effects of the β-hemolysin and enable deeper invasion of GBS into the tissue. Exogenous administration of surfactant has also been shown to limit bacterial growth and protect the lung (11, 13). The most prominent virulence factor is the outer capsule. The GBS capsule is composed of a capsular polysaccharide terminating in a sialic acid moiety (14, 15). Sialic acids can be joined to the preceding galactose in several different orientations involving the 2^{nd} carbon of sialic acid and either the 3^{rd} or 6^{th} carbon of galactose. The α2-3 sialic acid linkage is the most common type of linkage found in the GBS capsule (16), it is also identical to the most common sialic acid linkages found in the mouse and human lung (17). Sialic acids and the receptors they bind, the sialic acid-binding immunoglobulin-like lectins or Siglecs, form an important self-recognition pathway (18-20). Sialic acids are ubiquitously expressed throughout the body and dampen immune cell activation through ligation of these Siglec receptors (21). The inhibitory Siglec receptors recruit SHP phosphatases that dephosphorylate key intermediary kinases of the MAP kinase and NF-κB signaling pathways (22). The GBS capsule exploits this system of self-recognition to dampen host immunity and evade killing (23, 24). Lung macrophages express several different Siglec receptors, including Siglec-E and Siglec-F. A difference in expression of these Siglec receptors could enable GBS to persist in the lung by dampening host innate immune responses.

Another factor that could explain the enhanced susceptibility to GBS infection is the incomplete lung development at the time of infection in early-onset GBS infections. Lung development begins at embryonic day 9 (E9) in mice with the pseudoglandular stage involving the formation of the airways and the initial branching. The branching and airway development continue into the canalicular stage at E16 along with the initial vascularization

and angiogenesis in the lung. Beginning at E17 in the saccular stage, the alveolar sacs begin to form at the termini of the developing airways. The final stage of lung development is the alveolar stage where each alveolar sac is further subdivided into the final thin-walled mature alveoli (25, 26). This leaves a window between birth and the completion of lung development in which neonatal mice have reduced efficiency of gas exchange and are vulnerable to further tissue damage and reduced lung capacity, whereas adult mice have fully developed lungs.

In addition to the ongoing lung development, the fetal immune system is also developing. The earliest fetal immune cells begin migrating from the yolk sac blood islands around E7 of gestation. The population of fetal tissues with immune cells can be divided into 3 distinct 'waves'; the primitive, transient definitive, and definitive waves (27, 28). The primitive wave populates the fetal tissues with a F4/80^{hi}, CD11b^{lo} macrophage population termed primitive yolk-sac derived macrophages and are derived from myeloid precursors (MPs) in the yolk sac blood islands. The transient definitive wave consists of erythromyeloid precursors (EMPs) originating from the yolk sac, differentiating into fetal monocytes in the fetal liver and populating the fetal tissues beginning at E14. The definitive wave changes the site of immune cell maturation to the bone marrow and populates the tissues with long-lived tissue-resident macrophage precursors and hematopoietic stem cells (HSCs) (27, 28). Most tissue-resident macrophages are derived from this fetal monocyte population, excluding microglia which instead are derived from yolk-sac macrophages (29). These waves of hematopoiesis and seeding of tissue-resident immune cells result in the following populations being apparent in the lung: At E12 of gestation, the lung contains a population of F4/80^{hi}, CD11b^{lo} macrophages consistent with a primitive yolk sac-derived macrophage population found in other tissues, most notably the brain (30). At E14, a second population that is

F4/80^{lo}, CD11b^{hi} deriving from the fetal liver begins to appear in the fetal lung (31, 32). At E16, the bone marrow derived fetal monocytes appear in the lung, though it is believed that the fetal liver derived monocytes are the primary source of adult mature alveolar macrophages (31, 33, 34). Of the two main populations in the fetal lung, the yolk-sac macrophages and the fetal liver monocytes, the fetal liver monocytes are the more pro-inflammatory cell type and the most responsive to LPS (35). Indeed, the relative ratio of macrophages to monocytes favors macrophages perinatally as the fetal liver monocytes differentiate into pre-alveolar macrophage and eventually into alveolar macrophages (27) in the postnatal period. However, each population found in the fetal lung during development can differentiate into AMϕs to fill an empty niche in the case of a sudden loss of AMϕs, suggesting the importance of a tissue-derived factor influencing AMϕ development (36). The lung macrophages arising from these precursors form an integral part of immunity in the lung, especially in the postnatal period.

Alveolar macrophages are the major resident immune cells in the lung residing in the airways and protecting the lung after birth from inhaled pathogens. AMϕs can phagocytose and kill microbes, release inflammatory mediators, recruit additional immune cells including neutrophils, and participate in tissue repair following injury (37-39). AMϕs undergo a complex maturational process beginning in the fetal period. Fetal liver monocytes entering through the vasculature are exposed to GM-CSF in the interstitial space triggering the differentiation into a pre-AMϕ intermediate population. The pre-AMϕs then transmigrate into the alveoli where the concentration of GM-CSF is highest (40). Further exposure to GM-CSF results in the complete maturation of AMϕs at around PND3-4 (41). The AMϕ maturational process can also be tracked through observed changes in cell surface marker expression. The

major precursor cells of AMϕ are the F4/80^{int}, CD11b^{hi} fetal liver monocytes. During maturation, F4/80 expression increases while CD11b expression decreases. Additionally, CD11c and Siglec-F also begin to be expressed with CD11c expression being expressed at birth and Siglec-F not being expressed until PND3-4 (41). Expression of Siglec-F marks complete maturation into AMϕ. This AMϕ maturational process is driven by epithelial GM-CSF production and cell-autonomous TGF-β signaling (34, 42-44). The transcription factor, PPAR-γ is also critical for AMϕ maturation (45, 46). Loss of any of GM-CSF, PPAR-γ, or TGF-β blocks differentiation of the fetal liver monocytes into pre-AMϕ and subsequently AMϕ. Mice deficient in any of these factors develop pulmonary alveolar proteinosis due to the inability of the immature fetal monocytes to metabolize airway proteins and the subsequent accumulation of airway proteins (43, 45).

The other population of macrophages in the lung are the interstitial macrophages (IMϕ). The IMϕs are not as abundant in the lung and have not been studied as extensively as the AMϕs and thus the function or role of these IMϕs remains unclear (47). Recent work has further subdivided these IMϕs based on cell surface marker expression and location within the lung. Three distinct IMϕ populations could be identified from the non- AMϕ, defined as Siglec-F^{-}, compartment of the lung macrophages. The 3 different IMϕ differed in expression of MHC-II and CD11c, however, each of these 3 IMϕ populations displayed higher expression of pro-inflammatory genes including cytokines and receptors, as well as C1qa, C1qb, and C1qc, key components of the complement system (48). The IMϕs can also be subdivided based on location within the lung into BIMϕ or bronchial insterstitial macrophage and AIMϕ or alveolar interstitial macrophages. The BIMϕ had similar phagocytic ability as

AMϕ despite key differences in cell surface marker expression and the lack of expression of key phagocytic receptors found on AMϕ (48). These BIMϕ were hypothesized to originate from circulating monocytes due to the expression of key monocyte lineage genes (48). However, it is not well understood how the broader IMϕ population arises, whether it develops embryonically or postnatally.

Nerve and airway associated macrophages (NAMϕ) were also recently identified (49). These NAMϕ were found in the interstitial space surrounding larger airways and close to nerve bundles. Despite being found in the interstitial space, NAMϕ surface maker expression more closely resembles that of AMϕ. NAMϕ are F4/80^{hi}, CD11b^{lo}, CD11c^{int}, Siglec-F^{int}, as well as being Sialoadhesin (Sn)$^{+}$. NAMϕ express high levels of immunoregulatory genes and aid in dampening inflammation after infection. In an influenza model of infection, the NAMϕ quickly expanded via signaling through TLR3 and aided in tissue repair and return to homeostasis (49). Yet NAMϕ derive from the yolk sac and do not require GM-CSF for development or maintenance like AMϕ (49). The morphology of NAMϕ is also more resemblant of IMϕ, having dendritic-like projections and being more spindle shaped compared to AMϕ. The AMϕ, IMϕ, and NAMϕ each have important roles in maintaining lung homeostasis and deficiencies or immaturity of any of these populations could result in inabilities to kill GBS or to resolve lung pathology following infection.

Early-onset GBS disease results from aspiration of GBS into the lung during the birthing process. At the time of infection, neonatal mice have not completed lung alveolarization nor do they have fully mature AMϕ, the primary immune cells in the airway. Each of these differences in lung structure and immune cell populations between adults and

neonates could contribute to the overall susceptibility in neonates to severe GBS pneumonia. It is not well understood if human AMϕ are similarly immature as murine AMϕ are at birth. Newborn AMϕ may therefore lack the fully differentiated phenotype present in older children and adults (41). Apart from AMϕ, multiple other cell populations serve to protect the lung from infection and injury. Epithelial cells secrete surfactant and antimicrobial peptides capable of killing and/or inactivating inhaled microbes (50, 51). In addition, mucociliary clearance captures and removes particulates and infectious agents (52). The unique susceptibility of the neonate to severe GBS pneumonia and sepsis could implicate AMϕ immaturity and/or a deficiency in other components of lung immunity or lung structure.

Studies have focused on neonatal models of sepsis or on using adult genetic knockout mice to investigate neonatal susceptibility or key host factors in protective immunity against GBS. Studies in adult mice have revealed several key host factors involved in GBS immunity. GM-CSF deficient mice, lacking mature AMϕ, were more susceptible to GBS infections having higher recovered CFU and deficient cytokine production (53). This increase in CFU was tied to an inability to generate reactive oxygen species and an appropriate killing burst. The role of the pro-inflammatory cytokine IL-1β and the related inflammasome and signaling pathways were also investigated in the context of GBS infections. Loss of the IL-1R led to several downstream effects most notably neutropenia from decreased chemokine expression (54). While loss of MyD88 or any component of the inflammasome, NLRP3, ASC, or Caspase 1 led to severe GBS infection and increased mortality (55). A pair of studies in 2014 investigated the interaction of the GBS capsule with specific Siglec receptors, Sialoadhesin and Siglec-E (21, 56). The GBS capsule terminating in sialic acid engages both Sn and Siglec-E on host macrophages. Sig-$E^{-/-}$ mice had increased killing, phagocytosis, and cytokine

production. This was also apparent in the lung, where the Sig-E$^{-/-}$ mice had significantly elevated IL-1β and IL-6 with decreased IL-10 production (21). Though Sig-E$^{-/-}$ mice were susceptible to rampant inflammation and suffered increased mortality when given a larger inoculum of GBS (21). On the other hand, Sn$^{-/-}$ mice were unable to phagocytose GBS and thus had higher CFU recovered. Sn$^{-/-}$ mice also had reduced antibody titers, possibly a result of the combined effects of an inability to phagocytose GBS and present antigen coupled with observed deficiencies of antibody titers in Sn$^{-/-}$ mice (56, 57). Recently, a vertical transmission model of GBS infection was developed that closely mimics the natural route of infection observed in humans (58). In this study, the female mice were vaginally colonized with GBS and allowed to give birth. The newborn mice born to these mothers developed pneumonia progressing to sepsis and meningitis consistent with the observed progression of disease in humans. Initially, the neonates had significant lung pathology and CFU recovered from the lung (58). The hemolysin and cytolysin mutant, ΔcylE, failed to cause pathological changes in the lung, and was not recovered from the blood or liver. Additionally, the survivors of meningitis had long term cognitive decline in adulthood highlighting the potential severity of GBS infections (58). Though this model reflects the natural progression of GBS disease in neonates, it did not address what mechanisms allow for severe neonatal disease while leaving adults relatively unaffected. These studies provided a solid foundation of knowledge in GBS infections and mechanisms important for adults to kill GBS, but didn't address what mechanisms may be absent in neonates. Using these studies as a guide, we first sought to develop a model that would allow us to infect both adults and neonates and then test whether these mechanisms are deficient in neonatal mice.

There were several remaining questions that we sought to address. First, there were not any studies comparing adult and neonatal responses to GBS infections and so it was difficult to understand the mechanism of neonatal susceptibility to GBS without having a comparison from a relatively unaffected population. Second, most studies on GBS infections on neonates centered around neonatal sepsis. While GBS sepsis is a serious and devastating infection in newborns, we sought to first understand neonatal lung immunity and the differences that may exist between adult and neonatal lung immunity that could allow GBS to persist in the neonatal lung thereby enabling disease progression to sepsis and meningitis. Third, it wasn't well understood when this period of susceptibility to GBS ended or which milestones in neonatal development closed the window of susceptibility to GBS infections. Our strategy to address these remaining questions was to first develop a novel intranasal model of GBS pneumonia in neonates that was reliable, replicable, and recapitulated key aspects of GBS pneumonia in humans. Subsequently, to extend the use of that model to adults and juveniles, in a way that would allow comparisons back to the neonatal response, both to better understand the underlying mechanism of neonatal susceptibility and when the window of susceptibility closes.

Here we provide data from a neonatal mouse model that recapitulates many key aspects of human GBS disease, including the timing of mortality from lung disease and later-onset bacteremia and CNS involvement. We find that the inability of neonatal mice to kill GBS and resolve lung injury correlates to AMϕ immaturity at birth, and in particular a differential kinetic expression of two key lectin receptors (Siglecs) that bind the sialic acid-containing GBS exopolysaccharide capsule (CPS), an essential virulence determinant of the pathogen. Identifying a cellular basis of neonatal GBS susceptibility highlights principles of

developmental immunity and pathogen molecular mimicry potentially amenable to therapeutic targeting, with an eye to augmenting neonatal AMϕ development and closing a high-risk window for lethal GBS infections.

MATERIALS AND METHODS

Mice

Wild-type (WT) male and female C57BL/6 mice were obtained from Envigo and bred in house. Adult (8-10 weeks of age), juvenile (postnatal day 7, PND7), and neonatal (PND1, PND2, or PND3) were used. All animal experiments, including infections, were approved the University of California, San Diego Institutional Animal Care and Use Committee (IACUC). After infections, mice were monitored twice daily. Any mouse that lost >10% body weight or exhibited signs of severe disease or distress was humanely euthanized prior to the defined endpoint of the experiment.

Bacteria

The WT GBS strain used in all experiments was COH1, a highly encapsulated serotype III clinical isolate (23) with established virulence in murine models of pneumonia, sepsis and meningitis (21, 59, 60). All strains were propagated in Todd-Hewitt Broth (THB). COH1 was transformed with a GFP expression plasmid (erythromycin selection) to enable easier detection in the earlier time point pneumonia challenge studies. Isogenic, in frame allelic replacement mutants in the COH1 background lacking its capsular polysaccharide (ΔcpsD, aka HY106) or only the terminal sialic acid of the capsule side chain (ΔneuA) were also used, and their generation has been previously described (16, 61).

Pneumonia Model

Adult, juvenile, and neonatal mice were infected with a weight-adjusted inoculum of GBS so that immune responses could be compared between age groups. WT GBS (strain COH1) was used in the longer time points model (1, 3, and 7 days). A GFP-expressing GBS (strain

COH1) was used in the shorter time points model (0.5, 2, 6, 12, 24 h). Neonatal mice (PND1-PND3) were also infected with a larger inoculum, 100x more concentrated than the standard inoculum used. Survival was monitored over the course of 21 days and any animal showing signs of severe disease was humanely euthanized. An overnight culture of GBS in THB was sub-cultured and grown to mid-logarithmic phage (OD600 = 0.4). One ml of sub cultured GBS was then removed and washed with HBSS, centrifuged for 5 min at 5,000 RPM, the bacterial pellet resuspended in 1 ml HBSS, and serial dilutions performed to the desired inoculum. Due to the differing volumes of air space in the lungs between adults, juveniles, and neonates, in order to give equivalent doses of GBS to each age group the volume of the intranasal inoculum had to be adjusted. Adults were given 50 μl of GBS suspension intranasally, juveniles 10 μl, and neonates 2 μl. Adults weighed, on average, 5-fold times more than juveniles, and 25-fold more than neonates. Adults, juveniles, and neonates were anesthetized using 3% isoflurane. The corresponding amount of GBS suspension was then pipetted into the nares and aspirated. Animals were monitored until recovery from anesthesia.

Intraperitoneal Injections

To test possible therapeutic agents in neonatal GBS infections, pregnant mothers were gently restrained and injected intraperitoneally at E18 of gestation with either a vehicle control suspension or an interferon (IFN-α, IFN-γ) or either 0.1 or 0.5 mg rosiglitazone. The treated mothers were monitored twice daily for signs of distress following injection for 1 week total. After delivery, the neonates were also observed for signs of distress. The neonatal lungs were taken and analyzed by flow cytometry for Siglec receptor expression.

Cell Culture

To test potential therapeutic agents *in vitro*, PND2 neonatal lungs were digested into whole single-cell suspensions and pooled together. The pooled cells were then plated at a density of 1,000,000 cells/well in a 12-well plate. Each well was treated with a different agent for 8, 14, or 38 h after stimulation, LPS – 250 ng/mL, Pam3CSK4 – 300 ng/mL, GM-CSF – 10 ng/mL, TNF-α – 10 ng/mL, IFN-γ – 10 ng/mL. Following stimulation, the cells were removed from culture and stained for analysis by flow cytometry.

Bacterial Quantification

Bacterial counts were obtained by homogenizing the medial and caudal lobes of the lung in 1 ml HBSS. The resultant lung homogenate and serial 10-fold dilutions were plated on Todd-Hewitt agar (THA) plates, which were incubated at 37^{o}C for 24 h, at which point colony forming units (CFU) were enumerated.

Histology

The right lobes of the lung in adults, juveniles, and neonates were removed and fixed in 4% paraformaldehyde overnight. The following day, lung lobes were dehydrated via changes along an ethanol gradient. Paraffin embedding, sectioning, and hematoxylin and eosin (H&E) staining were all performed by the UC San Diego Histology Core at the Moores Cancer Center. Hematoxylin and eosin (H&E)-stained micrographs were captured using a Leica brightfield microscope and color CCD camera.

Lung Pathology Scoring

Adult, juvenile, and neonatal H&E stained micrographs were analyzed for interstitial inflammation, alveolar inflammation, alveolar collapse, bronchitis, and endothelitis. Each

category was scored 0-3 (absent, mild, moderate, severe) by 3 blinded independent reviewers. The scores were compiled and statistical analysis performed as below.

Flow Cytometry

The left lobes of adult, juvenile, and neonatal mice were processed and digested in RPMI containing 2 mg/mL of collagenase IV for 15 min. The resulting single-cell suspension was filtered and washed. Lung cells were stained with CD45 (BD Biosciences), CD11b (BioLegend), CD11c (BioLegend), CD64 (BioLegend), F4/80 (BioLegend), Siglec-F (BD Biosciences), Gr-1 (BioLegend), and MHC-II (BioLegend), Siglec-E (BioLegend), CD169/Sialoadhesin (BioLegend) for 30 min at 4˚C. Cells were then washed and resuspended in FACS buffer. The cells were analyzed by flow cytometry on a BD FacsCanto II using FlowJo software.

Cell Sorting

For ATAC-seq analysis, adult and PND4 neonatal mice were given intranasal PBS or LPS 2 h prior to euthanasia and lung dissection. The lungs were processed similarly as for flow cytometry analysis, except for digestion by Liberase (Roche). The resulting single-cell suspension was stained for 1 h on ice with CD45, CD11b, CD11c, F4/80, Siglec-F, and CD64. The stained cells were then sorted on a BD FACSAria II Cell Sorter. The sorted AMϕ were $CD45^{+}$ $F4/80^{hi}$ $CD11b^{lo}$ $CD11c^{+}$ Siglec-F^{+} $CD64^{+}$.

RNA Extraction and cDNA synthesis

The cranial and accessory lobes of adult, juvenile, and neonatal lungs were snap frozen in a bath of ethanol and dry ice for later RNA extraction. For extraction, the snap frozen lungs were suspended in 500 µl TRIzol reagent (Ambion) and homogenized using mechanical

pestle motor. An additional 500 µl TRIzol was added and the homogenate kept at room temperature for 5 min prior to addition of chloroform for extraction of RNA. There, the upper aqueous layer was washed with isopropanol and ethanol, and RNA suspended in molecular grade water for quantification on a NanoDrop spectrophotometer. cDNA synthesis was performed using a Superscript III Reverse Transcription Kit (Invitrogen) according to the manufacturer's protocol.

qPCR

qPCR reactions were run on a BioRad CFX96 Touch Real-time System for 40 cycles. Briefly, each reaction consisted of 16 µl of SYBR green (BioRad), 9.44 microliters of µl grade H2O, 6.4 microliters of forward and reverse primers (sequences listed below, Integrated DNA Technologies), and 0.16 microliters of cDNA. Each reaction was added in triplicate, 10 µl per well.

Immunofluorescence and Confocal microscopy

The left lobes of adult, juvenile, and neonatal mice were removed and briefly fixed in 4% paraformaldehyde for 1 h at room temperature. Following fixation, lungs were washed in PBS containing Ca2+ and Mg2+ and put in 15% sucrose until they sank to the bottom. Afterwards, the lungs were placed in 30% sucrose for 6 h, then frozen in optimal cutting temperature (OCT) compound and placed into a cutting mold. The frozen blocks were sectioned at the UC San Diego Moores Cancer Center Histology Core. Each frozen slide was briefly fixed in 2% paraformaldehyde for 20 min then permeabilized with Triton-X100 for 5 min. A blocking solution containing 5% each donkey and goat serum was added to each slide for 1 h. Following blocking, the primary antibody solution containing 1% BSA and 0.1% Triton-

X100 along with anti-CD68 (OriGene) and anti-GBS (Abcam) primary antibodies was added and incubated overnight. In other experiments, fluorescently conjugated anti-CD68 (BioLegend) and anti-CD169/Sialoadhesin (BioLegend) antibodies were used in conjunction with the anti-GBS primary antibody (Abcam). The next day, each slide was washed thoroughly before the secondary antibody solution was added, containing anti-rat AlexaFluor-488 and anti-rabbit AlexaFluor-555, for 2 h. A DRAQ5 (ThermoFisher) solution was added for 25 min. Following staining, each slide was dried before a ProLong Gold anti-fade mountant (Life Technologies) was added dropwise. In some experiments, ProLong Gold anti-fade mountant with DAPI (Life Technologies) was added. Each slide was cured overnight. The next morning, each slide was sealed and imaged using a Leica TCS-SPE Confocal microscope at 100X, 400X and 630X magnification. For 4 color images, a Leica SP5 Confocal microscope at the UCSD Microscopy Core was used to image slides at 630X magnification.

Human lung macrophage gene expression

Human studies were reviewed and approved by the Institutional Review Board at the University of California, San Diego and Rady Children's Hospital. Tracheal aspirate macrophages were obtained via endotracheal suctioning as part of routine respiratory care of intubated and mechanically ventilated patients born before 30 weeks gestation. Samples were obtained within the first 24 h of life and again on day 7. Macrophage RNA was isolated by TRIzol extraction and gene expression measured using Affymetrix GeneChip Human Transcriptome 2.0 Arrays.

ATAC-seq Library Preparation

Following sorting, 50,000 AMϕ were washed with PBS followed by cold lysis buffer (10 mM Tris-HCl, pH 7.4, 10 mM NaCl, 3 mM MgCl2, 0.1% IGEPAL CA-630). After centrifugation, the cell pellet was resuspended in 50 ml 1X reaction buffer (25 mL Tagment DNA Buffer, 2.5 mL Tagment DNA enzyme I, and 22.5 mL water) (Nextera DNA Library Preparation Kit, Illumina). Transposase reactions were performed at 37^{o}C for 30 minutes. Following the reaction, DNA was purified using ChIP DNA Clean & Concentrator kits (Zymo Research). DNA was amplified using the Nextera primer Ad1 and a unique Ad2.n barcoding primer using NEBNext High-Fidelity 2XPCR Master Mix (NEB) for 14 cycles. The libraries were then restricted to 175-225 bp and single end sequenced using a HiSeq 4000 or a NextSeq 500 (Illumina) for 51 cycles according to the manufacturer's instructions. Protocol adapted from (62).

Statistics

All statistical analyses were performed using GraphPad Prism 6. P-values < 0.05 were considered statistically significant and denoted with a single asterisk. P-values < 0.01 were denoted with two asterisks, P-values < 0.005 were denoted with three asterisks, and P-values < 0.001 were denoted with four asterisks. Experiments quantifying GBS bacteria and comparing cell surface expression were analyzed using the non-parametric Mann-Whitney U test. Experiments depicting the fold-change in mRNA expression were analyzed using the ΔCT values between the gene of interest and the housekeeping gene GAPDH, and evaluated using the parametric unpaired t test.

RESULTS

Increased Mortality and Persistence of Lung Injury in Neonatal GBS Infection

Despite being the most common cause of neonatal pneumonia, the molecular and cellular mechanisms responsible for the unique susceptibility of newborns to GBS remain unclear. To investigate key host-pathogen interactions in the newborn period, we developed and employed a murine model of GBS neonatal pneumonia (see Materials and Methods). Newborn C57BL/6 mice were lightly anesthetized and intranasally inoculated with 28,000 CFU/g of wild-type (WT) GBS (serotype III strain COH1). Control mice were similarly anesthetized and received an identical volume of sterile, endotoxin-free saline. For comparison, we also infected juvenile (PND7) and adult (8-week-old) mice with a comparable weight-based GBS inoculum. Adult and juvenile mice universally survived infection (Figure 1A). However, in neonatal mice, over 20% of GBS-infected animals died within 2 days. We did not observe additional deaths in any group between days 2 and 7.

We cultured GBS from infected lungs to compare bacterial clearance between neonatal, juvenile, and adult mice (Figure 1B). Adult mice did have viable GBS bacterial CFUs in their lungs 1 day after infection but no GBS when measured at day 3. Two adult mice did have rare detectable GBS on day 7 after infection. Juvenile and neonatal mouse lungs contained viable GBS when measured both 1 and 3 days after infection. We next measured temporal changes in lung pathology following GBS infection. All ages of mice infected with GBS developed histological signs of significant acute lung injury 1 day following infection (Figures 1C and 1D). However, adult mice infected with GBS showed rapid histological improvement by day 3 and complete resolution by day 7. By comparison, abnormal pathology in GBS-infected juvenile mice persisted to day 3 with resolution by day 7. Pathology in GBS-infected neonatal

mice was even more persistent, with no improvement as late as 7 days post infection. Our GBS infection model therefore replicates the clinical scenario of early-onset GBS disease, which includes severe pneumonia, lung injury, and death specifically in neonates. In addition, these initial experiments suggest neonates have defects related to clearance of GBS and resolution of lung injury.

Delayed Kinetics of Lung Inflammation and GBS Clearance by Alveolar Macrophages in Neonatal GBS Pneumonia

The very distinct differences in GBS clearance and resolution of lung pathology between newborn and adult mice suggested potential differences in the lung immune response and inflammatory signaling. To initially test the innate immune response to GBS, we measured expression of pro-inflammatory mediators *Il1b*, *Il6*,and *Cxcl1* in the first 24 h following GBS infection. Adult mice had elevated levels of each inflammatory mediator during the 2- to 12-h time window following GBS infection; however, expression levels of the factors fell back to baseline by 24 h (Figure 2A). By contrast in neonatal mice, expression of *Il1b*, *Il6*, and *Cxcl1* did not increase until 24 h after GBS infection (Figure 2B), revealing a delayed inflammatory response in neonatal mouse lungs compared with adults. Adult lungs had a rapid influx of additional $CD68^+$ macrophages and monocytes into the lung 12–24 h after GBS inoculation; however, neonatal lungs did not show such an accumulation of $CD68^+$ cells 24 h after infection (Figure 2C). This finding corresponded to the delay in the upregulation of key inflammatory mediators and chemoattractants. Thus the neonatal lung immune response to GBS pneumonia is delayed, both in terms of inflammatory mediator production and the accumulation of $CD68^+$ myeloid cells. We next tested if the delayed inflammatory response in neonates impaired GBS clearance by measuring viable GBS throughout the first 24 h

following infection (Figure 2D). In adult lungs, the number of GBS CFU recovered fell steadily over the first 24 h. Juveniles had less dramatic but still significant reductions in CFU by 24 h. However, neonatal mice were not able to reduce GBS CFU counts during the first 24 h following infection, consistent with an inherent defect in killing GBS during the newborn transition. These findings suggested that early in the disease process in vivo, neonatal AMϕ lacked the ability to phagocytose and kill GBS. As juvenile mice achieved partial GBS clearance to prevent persistent lung pathology, we more closely examined how long the window of susceptibility to GBS persisted in newborn mice. For these experiments, mice were infected with a higher inoculum of intranasal GBS on days 1, 2, or 3 of life (Figure 2E). Survival depended on day of infection, and 50% of mice infected on day 1died within the first 24 h. Mice infected on day 2 survived the initial acute period but suffered late mortality between days 11 and 14. In contrast, all mice infected on day 3 of life survived for at least 21 days. When survivors were sacrificed 21 days following infection, we detected significant intrapulmonary GBS only in mice infected on day 1. In subsets of mice infected on day 1 but surviving until day 21, GBS had also spread to the spleen. These findings suggested that mice infected with GBS within the first day of life have reduced survival and lack the ability to adequately clear GBS in the lung and prevent systemic dissemination of the pathogen. Newborn mice apparently acquire the ability to control GBS and protect against devastating infection within the first several days of life. Confocal microscopy identified potential differences in cellular interactions following GBS infection (Figure 2F). In adult lungs, $CD68^+$ AMϕ localized to the sites of GBS infection within the first 2 h. By 12–24 h, the majority of GBS visualized in adult lungs were inside $CD68^+$ macrophages, consistent with active phagocytosis. These data correlated with CFU kinetics, where the vast majority of

viable GBS were cleared from adult lungs within 24 h after infection. In juvenile lungs, AMϕs accumulated around the sites of GBS infection within the first few hours, and some AMϕs were seen to phagocytose GBS. However, by 24 h after infection, substantial quantities of noninternalized GBS were still observed throughout the lung parenchyma, even in areas of AMϕ accumulation. We documented a very different pattern in neonatal lungs. GBS were distributed throughout the lung but also occasionally accumulated in small masses within the airways. AMϕ in these regions surrounded the GBS, but with very little evidence of phagocytic uptake. These data were consistent with CFU data showing lack of significant GBS clearance in neonatal lungs over the first 24 h following infection.

Mature AMϕs Are Required for Rapid GBS Clearance

In the lung, AMϕs provide the major initial response to inhaled or aspirated microbial pathogens. In adults, inflammatory stimuli or lung injury increase expression of CD11b on fully differentiated, Siglec-F^+ AMϕs (63, 64). We measured a similar increase in CD11b expression on adult Siglec-F^+ AMϕ beginning on the first day after GBS infection with return to baseline levels by day 7 (Figures 3A, S2). Juvenile AMϕ also increased CD11b on day 3 after GBS infection. However, AMϕ in GBS-infected neonatal mice, which did not express Siglec-F until day 3 of life, also did not show a measurable increase in CD11b expression. Therefore, although GBS infection did not interfere with AMϕ acquisition of Siglec-F expression, immature AMϕ within the neonatal lung did not display the same changes in differentiation marker expression as adult cells. We hypothesized that AMϕ maturity determined either protection against GBS in adults or susceptibility to GBS in neonates. To initially test the requirement of mature AMϕ, we depleted AMϕ from adult mice using

liposomal clodronate prior to GBS infection. Intranasal administration of clodronate liposomes reduced the number $CD11c^{+}$ Siglec-F^{+} AMϕ (Figures 3B, S3). We then infected both clodronate-treated adult mice and controls treated with empty liposomes. By 24 h after GBS infection, confocal imaging of clodronate-treated mice infected with GBS did demonstrate small, $CD68^{lo}$ monocytic cells in the lung after GBS infection, but these cells were not efficient at phagocytosing bacteria (Figure 3C). Clodronate-treated adults had significantly higher GBS CFU recovered from the lungs compared with control adults (Figure 3D). Consistent with the requirement of AMϕ maturation, newborn $Csf2^{-/-}$ mice, which lack fully differentiated AMϕ (41, 43), had higher levels of GBS within their lungs 24 h after infection (Figures 3E and 3F).

Developmental Maturation of Lung Myeloid Siglec Expression

The heavily sialylated capsule of GBS contributes to bacterial virulence. In hosts, the sialic acid-binding immunoglobulin-type lectins Sialoadhesin (Sn) and Siglec-E both bind GBS sialic acid moieties (21, 56). GBS sialic acid binding to Siglec-E reduces the proinflammatory innate immune response to GBS (21). In adult mice, Sn mediates GBS phagocytosis and killing (56). Given the dramatic defects we measured in neonatal mouse lung macrophages, we next examined the developmental dynamics of Siglec-E and Sn expression in lung myeloid populations by FACS (Figure 4; Table S2). In adult lungs, Sn expression was detected in AMϕ (both $CD11b^{hi}$ and $CD11b^{lo}$) and in recently described $CD11c^{-}$ nerve and airway-associated macrophages (NAMϕs (49); Figures 4A). Clodronate depletion of AMϕs significantly reduced lung Sn expression (Figure S3). Adult neutrophils (PMNs) and interstitial macrophage/monocyte and dendritic cell populations (IMϕ and IMϕ/DC) were Sn-

negative. Siglec-E expression was slightly more widespread in adults, being expressed in AMϕs, NAMϕs, neutrophils, and to a lower level in $CD11c^+$ IMϕ/DC cells. Sn and Siglec-E expression in juvenile lung myeloid cells closely resembled the patterns observed in adults (Figure 4B). The neonatal lung contains PMN, IMϕ, and developing AMϕ populations (Figure 4C). Sn expression was only detected in AMϕ, whereas Siglec-E was measured in all populations. Overlaying FACS detection of Sn and Siglec-E in all $CD45^+$ cells (Figures 4D and 4E) and all $F4/80^+$ $CD11b^+$ macrophages (Figures 4F and 4G) illustrated the reduced Sn expression in the neonatal lung compared with juveniles and adults. Backgating analysis of the $F4/80^+$ $CD11b^+$ macrophages revealed that Sn expression was limited to $F4/80^{hi}$, $CD11b^{lo}$ AMϕs, while Siglec-E was expressed in both subpopulations of the $F4/80^+$ $CD11b^+$ macrophage gate (Figure S3). However, expression of the inhibitory Siglec-E was similar across all three timepoints tested.

Developmental Immaturity of AMϕ Siglec-Sialic Acid Detection Contributes to Neonatal GBS Susceptibility

We further investigated the potential contribution of developmental immaturity of Sia receptor expression in neonatal lungs to the inability to rapidly clear GBS. Real-time PCR and immunostaining demonstrated consistently lower Sn expression in newborn mouse lungs (Figures 5A and 5B). We then leveraged a recently completed study examining gene expression in preterm infant tracheal aspirate macrophages to test the dynamics of Sn expression in humans. Samples obtained on the first day of life had lower *hSIGLEC1* (Sn) compared with samples obtained on day 7 (Figure 5C). Expression of *SIGLEC9* (the human paralog of Siglec-E) was similar at these two timepoints. We next tested if deletion of the inhibitory Siglec-E could remove a potential defect in GBS killing. In adult mice (which

express high levels of Sn), Siglec-E deletion had no effect on GBS killing (Figures 5D and 5E). However, newborn SigE$^{-/-}$ mice showed improved GBS killing compared with WT controls with fewer colonies of bacteria isolated from the lungs 24 h after infection (Figure 5F). Confocal microscopy identified increased GBS phagocytosis in newborn SigE$^{-/-}$ lungs compared with controls (Figure 5G). Therefore, removal of the inhibitory Siglec-E improved GBS phagocytosis and killing by neonatal AMϕ even in the setting low Sn expression. In Csf2$^{-/-}$ mice that lack normal AMϕ differentiation, we detected even lower neonatal Sn expression on lung macrophages compared with WT neonatal mice (Figure 5H). Adult Csf2$^{-/-}$ AMϕ lacked Siglec-E expression, whereas expression in neonates was similar (Figure 5I). Therefore, in both mice and humans, immature newborn AMϕ have adult levels of the inhibitory receptor Siglec-E but lack expression of Sn. Alterations of the GBS capsule to eliminate sialic acid also improved clearance in the neonatal lung. We infected mice with GBS strains bearing mutations in genes critical for either sialic acid modification (ΔneuA) or capsule formation (ΔcpsD). Although clearance in adults was similar to WT GBS (Figures 5J and 5K), newborn mice showed improved phagocytosis and killing of both ΔneuA and ΔcpsD strains (Figures 5L and 5M), confirming that the sialic acid-rich GBS capsule is a key virulence factor in the neonatal lung.

Sn expression declines over time following GBS infection

Increases in Sn expression over the first few days of life, from being absent at PND0, seemingly correlated with improved resistance to GBS infection as PND3 neonates universally survived the larger inoculum infection while the PND1 and PND2 neonates each developed severe disease and died at different stages of the infection. Following the apparent

importance of Sn expression in limiting GBS pneumonia, we were interested in how Sn expression is regulated following GBS infection. We utilized whole lung RNA collected from the 24 hour GBS infection model in Figure 2 and analyzed expression by real-time PCR of *Siglec1* (gene name of Sn) and *Siglece* (gene name of Siglec-E) at 0.5, 2, 6, 12, and 24 h following GBS infection in adults and neonates. Our initial hypothesis was that *Siglec1* expression would increase following GBS infection to allow for rapid phagocytosis and killing. However, *Siglec1* expression decreased in both the adults and the neonates. The decrease began at 0.5 h in the neonate (Figure 6B), and at 6 hours after infection in the adult (Figure 6A). When combining the adult and neonatal *Siglec1* expression, adults had significantly higher expression at 0.5 and 2 hours, but lost significance over the neonates at 6 and 12 hours, before trending upward towards baseline expression at 24 hours (Figure 6E). In contrast to *Siglec1* expression, *Siglece* expression remained relatively consistent throughout the infection period in both adults and neonates (Figure 6C, 6D). Adults trended towards increased expression at 2 and 12 hours. GBS infection did not alter expression of *Siglece*; adult and neonatal expression of *Siglece* during the infection period remained similar to expression at baseline (Figure 6F).

The Sia-Siglec-E interaction mediates decreased Sn expression following infection

We next wanted to test the importance of the sialic acid-Siglec-E interaction on Siglec receptor expression during infection. To do this, we compared the expression of *Siglec1* and *Siglece* from WT adults and neonates to adults and neonates infected with the sialic acid mutant GBS, ΔneuA at 0.5, 6, and 24 hours after infection. Adults infected with ΔneuA GBS had consistent expression of *Siglec1* throughout the infection period with significantly higher expression at 6 hours after infection over the WT GBS infected adults (Figure 7A). Neonates

also had consistent expression of *Siglec1* throughout after infection with ΔneuA GBS, with significantly higher expression over the WT GBS infected neonates at 6 hours (Figure 7B). *Siglece* expression was similar between WT and ΔneuA GBS infected adults and neonates with one notable exception (Figure 7C, 7D). At 6 hours after infection in the adult, the ΔneuA GBS infected animals trended towards increased expression of *Siglece*. Whereas in the neonates, the ΔneuA GBS infected animals had significantly decreased expression of *Siglece* compared to the WT GBS infected animals. Additionally, we measured cell-surface Sn and Siglec-E receptor expression via flow cytometry in neonatal Sig-E$^{-/-}$ mice 24 hours after infection with WT GBS or with saline control. WT neonates had reduced surface expression of Sn at 24 hours after infection but increased surface expression of Siglec-E (Figure 7E, 7F). Sn expression remained consistent in the Sig-E$^{-/-}$ neonates (Figure 7E). Taken together, the GBS Sia-Siglec-E ligand-receptor interaction mediates decreased Sn expression following infection.

We also wanted to investigate the cytokine response in adults and neonates infected with the ΔneuA GBS. GBS uses its sialic acid capsule to evade host immunity and dampen immune responses via engagement of host inhibitory Siglec receptors. Therefore we hypothesized that the animals infected with the ΔneuA GBS would have enhanced cytokine responses during the infection period. Adults infected with ΔneuA GBS had significantly higher expression of *Il1b* at 6 hours than did the adults infected with WT GBS (Figure 7G). We were unable to detect a similar increase in expression of *Il1b* in ΔneuA GBS infected neonates in the tested timepoints (Figure 7H). It is possible that peak *Il1b* expression in ΔneuA GBS infected

neonates occurs during a timepoint not tested here, which would indicate an earlier cytokine response than the WT GBS infected neonates that showed peak expression at 24 hours.

Siglec1 is Regulated by the STAT Pathway and is Differentially Accessible in the Adult

After establishing the importance of Sn in the early response to GBS infection, we hypothesized that increasing Sn expression on neonatal AMϕs would confer resistance to GBS infections and could therefore be used as a possible therapeutic intervention. We first sought to understand how *Siglec1* is regulated. Using 3 different online transcription factor databases, ChIPBase v2.0 (65), ImmGen Enhancer Networks, and ConTra v3 (66), we searched for transcription factor binding sites (TFBSs) within the promoter region of *Siglec1* and *Siglece*. ChIPBase v2.0 compiles Chromatin Immunoprecipitation Sequencing (ChIP-seq) data sets, cross-referencing TFBSs of transcription factors across hundreds of genes and building predicted regulatory networks (65). ConTra is a web tool that combines several different transcription factor databases (TRANSFAC, Jaspar) and allows the user to search any gene against those databases to find putative TFBSs. Users can also see how gene regulation may be conserved between different species (66). STAT1, STAT6, and IRF1 were common hits of multiple databases (Figure 8A) and were frequently shown to be involved in increased Sn expression in the literature (67-69). ConTra v3 depicts the promoter and UTRs of the gene of interest and searches those regions for TFBSs of selected transcription factors. In this case, both *Siglec1* and *Siglece* show repeated STAT6 and C/EBPα binding sites spread throughout the promoter and UTRs (Figure 8B). The chromatin state of genes also plays an important role in gene expression; ‘closed’ chromatin can silence genes while open chromatin allows for gene expression. Utilizing an Assay of Transposase Accessible Chromatin through

Sequencing (ATAC-seq) data set from sorted AMϕ in our lab, we assessed the chromatin states of the *Siglec1* and *Siglece* genes in PBS or LPS treated adults or PND4 neonates. One of the most differentially accessible sites in adults compared to PND4 neonates was a *Siglec1* site (Figure 8C), no such sites were found in the *Siglece* gene. Apart from that one site, neither *Siglec1* nor *Siglece* had any other discernible differences in number of peaks or peak height between the adults and PND4 neonates (Figure 8D). *Siglec1* is regulated by several different STATs and IRF1, key signaling TFs in the JAK/STAT pathway and downstream of the IFN receptors. Thus, exogenous interferon could increase Sn expression and be a potential therapeutic. The chromatin accessibility of the *Siglec1* gene locus is somewhat similar between adults and PND4 neonates, though with one site being among the top differentially accessible sites in the adult.

RG, IFN-α,γ Did Not Increase Sn Expression on the First Day of Life

Following our search of online transcription factor and gene regulation databases as well as other reports in the literature, we sought to test whether activators of these transcription factors could increase cell surface Sn expression on neonates. PND2 neonatal whole lung cells were cultured in the presence of Pam3CSK4, TNF-α, GM-CSF, LPS, or IFN-γ for 8, 14, or 38 h. These agents were selected because of their known roles in activating the NF-κB pathway (p65; Pam3CSK4, TNF-a, LPS), the STAT1/IRF1 pathway (LPS, IFN-γ), or are known to be involved in AMϕ maturation (GM-CSF) and could be involved in signaling through PPAR-γ. There was no discernible difference in Sn expression at 8 h of culture, and a small increase in Sn expression at 14 h of culture with LPS and IFN-γ (Figure 9A). At 38 h of culture, LPS, IFN-γ, and GM-CSF clearly increased Sn expression (Figure 9A). Interestingly,

there was large discrepancy in Sn expression between cells cultured with Pam3CSK4 and LPS despite both being TLR ligands and seemingly signaling through MyD88 and NF-κB. LPS in addition to signaling through MyD88 and the NF-κB pathway, also can signal through an alternative pathway involving TIRAP, ultimately resulting in the phosphorylation of STAT1 (70, 71). Thus, each of the agents that increased Sn expression shared a common capability of signaling through the JAK/STAT pathways. Moving towards *in vivo* testing, we focused on testing the interferons, IFN-γ and IFN-α. Because of the delay in achieving increased cell surface Sn expression and the relatively narrow window to provide effective intervention against GBS infections, we tested intraperitoneal (IP) injections of IFN-γ, IFN-α, or the vehicle control at E18 in an effort to increase neonatal Sn expression prior to birth and the beginning of the susceptibility window (Figure 9B). At PND0, there was no discernible increase in Sn expression on neonatal macrophages after prenatal administration of IFN-γ or IFN-α (Figure 9C). Siglec-F expression was also measured and analyzed to test whether AMϕ maturation would also be accelerated by IFN treatment, however IFN did not increase Siglec-F expression either (Figure 9C). The IFN-treated neonates did not survive beyond PND0 thus were unable to measure Sn expression at PND2 or PND4. Earlier we found that $Csf2^{-/-}$ adults did not express Sn or Siglec-E suggesting that AMϕ maturation is necessary for Sn expression. We then tested the PPAR-γ agonist, rosiglitazone at 2 different doses *in vivo* again via IP injection at E18. At PND0 there was no increase in Sn after either 0.1 or 0.5 mg rosiglitazone, though there was increased expression of Siglec-F at both doses, perhaps indicative of accelerated AMϕ maturation consistent with the known importance of PPAR-γ in AMϕ maturation (Figure 9D). At PND4 there was a small increase in Sn in the neonates

that received 0.1 mg rosiglitazone prenatally, though not at the 0.5 mg dose (Figure 9E). Siglec-F expression was still greatest in the neonates that received 0.1 mg rosiglitazone prenatally (Figure 9E). The higher 0.5 mg dose of rosiglitazone also exhibited toxicity, with mortality and growth retardation observed. Each of these different agents had different effects on the myeloid cell populations, seen by the CD11b x F4/80 flow cytometry plots. IFN-γ treated neonates had increased $CD45^+$ $F4/80^-$ $CD11b^+$ neutrophils, while IFN-α treated neonates had massively increased $CD45^+$ $F4/80^-$ $CD11b^-$ cells, perhaps indicating an increase in lymphoid cells. The lower dose of rosiglitazone had increased $CD45^+$ $F4/80^+$ $CD11b^+$ macrophages (Figure 9F, 9G). Although lower doses of rosiglitazone apparently increased Sn expression at PND4, an optimal increase of Sn expression would occur earlier in the window of susceptibility to severe GBS infection to maximize the therapeutic benefit.

Sialic Acid is Not Expressed in the Developing Fetal Lung

Previously in Figures 4 and 5, we found that Siglec-E is the only Siglec receptor expressed by neonatal macrophages. Siglec-F, commonly used as a marker of AMϕ maturation, is not expressed until PND3-4, while Sialoadhesin is not expressed at birth but increases steadily thereafter. Following this discovery, we began to explore what possible effects Siglec-E expression could have on developing AMϕs. Siglec-E is an inhibitory member of the sialic acid binding, immunoglobulin-like lectin superfamily; ligation of Siglec-E by α2-3 linked sialic acid expressing cells or proteins signals through an ITIM domain to recruit SHP-1,2 phosphatases. Ultimately resulting in dephosphorylation of key downstream kinases in the NF-κB and MAPK signaling pathways. We hypothesized that sialic acids present in the lung during gestation interact with fetal pre-AMϕs and ultimately regulate AMϕ maturation via

engagement of Siglec-E. We first wanted to assess the sialylation state of the lungs at different developmental stages from fetal (embryonic day 15, E15), neonatal (PND1), juvenile (PND7), and adult lungs as it was not clear from the literature at what mouse lung developmental stage sialylation of surface glycoproteins occurs. In humans, lungs appeared to lack terminal sialic acid residues during fetal development (72). To answer this question, frozen lung sections were stained for CD68 and either α2-3 sialic acid using *Maackia amurensis* agglutinin or α2-6 sialic acid using *Sambucus nigra* agglutinin. We only detected α2-3 sialic acid on discrete cells, but not the respiratory epithelium, in the neonatal, juvenile, and adult lung sections (Figure 10A). There was no observed staining in the fetal lung. In agreement with other reports (73), we did not observe any α2-6 sialic acid in fetal, neonatal, juvenile, or adult lungs (Figure 10B). Without expression of sialic acid by the lung epithelium or other immune cells in the lung, the sialic acid must come from outside the lung.

Loss of THP Alters Neonatal Siglec-E and Siglec-F Receptor Expression

Due to the lack of cellular sialic acid staining in the fetal lung, we tested the possibility of Tamm-Horsfall Protein (THP), an excreted sialylated glycoprotein in urine and therefore amniotic fluid, being the source of sialic acid in the lung. THP expresses the α2-3 sialic acid linkage and produced only in the thick ascending limb of the Loop of Henle in the kidneys. THP dampens inflammatory responses in neutrophils and binds Siglec-9 exclusively in humans and Siglec-E in mice (74). THP is also expressed relatively early in development by the kidneys. Therefore, we hypothesized that THP produced by the fetal kidney is excreted into the amniotic fluid which is then aspirated into the lungs where the sialylated THP interacts with fetal pre-AMϕs via the Siglec-E receptor (Figure 11A). To confirm the presence

of THP in the fetal lung, we performed an ELISA on several different fetal and neonatal tissues, including amniotic fluid samples, at E15 and PND1. Each fetal lung and liver sample tested positive for THP, while a subset of amniotic fluid samples had relatively high concentrations of THP (Figure 11B). THP was not detected in the PND0 neonatal lung samples (Figure 11B). To confirm these results and determine the localization of THP in the lung, we stained fetal lung sections for CD68 and THP. At E15, THP was observed in larger conducting airways and along the periphery of the tissue (Figure 11C, 11D). We next wanted to test whether the loss of THP impacted pre-AMϕ development. With little sialic acid expressed by fetal lung cells, the aspirated THP could provide the main source of sialic acid in the fetal lung. Using flow cytometry, we measured cell surface expression of Siglec-E, Siglec-F, and Sn on $CD45^+$ $F4/80^+$ $CD11b^+$ pre-AMϕs. At PND1 the $THP^{-/-}$ neonates had a separate Siglec-E^{lo} population. At PND2, this population was less distinct. By PND8, there was no discernible separate Siglec-E^{lo} population (Figure 11E). Though at each day tested, the $THP^{-/-}$ mice had a significantly lower median fluorescent intensity of Siglec-E than did the WT mice (Figure 11F). At PND2, the $THP^{-/-}$ mice also had a significantly higher median fluorescent intensity of Siglec-F, perhaps indicating a more rapid maturational process (Figure 11F). There was no detectable difference in Sn expression between the $THP^{-/-}$ and WT mice at any of the days tested (Figure 11F). The increase in Siglec-F expression coupled with the decrease in Siglec-E expression may represent a more pro-inflammatory subset of AMϕ better able to respond to neonatal infections.

We found that the fetal lung does not express either the α2-3 or α2-6 sialic acid, though the sialylated THP was detected in the lung and amniotic fluid at E15. However, THP was not

detected after birth. The PND1 THP$^{-/-}$ neonates appeared to have a Siglec-E^{lo}, Siglec-F^{+} pre-AMϕ population. This population did not persist, as PND8 THP$^{-/-}$ juvenile mice did not have a separate Siglec-E^{lo}, Siglec-F^{+} population, though at that stage AMϕ maturation has completed and that early Siglec-E^{lo}, Siglec-F^{+} may represent AMϕs that have undergone accelerated maturation in the absence of sialic acid-Siglec-E signaling. These early Siglec-E^{lo}, Siglec-F^{+} macrophages may also be more pro-inflammatory and less prone to GBS-Sia-Siglec-E mediated inhibition. The THP-Siglec-E interaction during gestation may be a key regulator of AMϕ maturation and development and could shape early neonatal immune responses to infections.

DISCUSSION

Prior to this work, it was unknown why neonates develop severe GBS disease and adults did not. Here, using a novel neonatal mouse model of GBS pneumonia, we show that PND1 neonatal mice develop severe pneumonia and lung pathology after infection. The adult and juvenile mice did not develop the same pathology and were able to efficiently phagocytose and kill the sialylated GBS. In the first few days of life, neonates do not have fully mature AMϕ and do not express a key sialic acid binding receptor, Sialoadhesin. The lack of expression of Sn, combined with adult levels of expression of the inhibitory Siglec, Siglec-E, creates a narrow window of susceptibility in which GBS can cause severe disease in neonates. This window is open at birth and gradually closes as Sn expression increases over time. With Sn expression being critical to resistance to GBS infection, we further investigated the regulation of Sn expression. The GBS sialic acid-Siglec-E ligand-receptor interaction mediates downregulation of Sn during GBS infection. Seeking possible therapeutic avenues to close the window of susceptibility to GBS infection prior to birth, we tested several different agents but were unable to increase Sn expression *in vivo*. Further investigation revealed tight regulation of the *Siglec1* gene via chromatin accessibility and remodeling in the first few days of life that may prevent Sn from being expressed early either naturally or via induction. While investigating the potential role of fetal Siglec-E expression, we uncovered a possible layer of fetal immune regulation via the sialylated Tamm-Horsfall protein. THP is produced in the kidneys and excreted in the urine, ingestion and aspiration of the sialylated THP could provide a systemic source of sialic acid that dampens inflammation and protects organ development, but also creates susceptibilities to postnatal infection. These two layers of fetal and neonatal AMϕ regulation, the Sia-Siglec-E interaction as well as the chromatin state of

key genes warrant future investigation to identify ways to modulate the regulation and confer greater resistance to neonatal infections.

Like many human pathogens, GBS expresses a variety of virulence factors to subvert host immune detection and killing and/or promote cellular damage (11, 75). However, the same GBS strains that asymptomatically colonize adults can cause devastating disease in newborns. We hypothesized that the neonatal window of susceptibility is primarily due to defective maturation of host pulmonary innate immunity. In addition to AMϕ function, lung immunity includes antimicrobial peptides, surfactant, mechanical mucus clearance, resident lymphocyte and dendritic cell function, and neutrophil influx (76-78). Although our data here do not discount important contributions of these or any other mechanisms, rapid GBS clearance was impaired in mice depleted of AMϕs and in $Csf2^{-/-}$ mice that lack mature AMϕs. Our data also clearly demonstrated that neonatal AMϕ lack sufficient expression of Sn for effective detection, phagocytosis, and killing of sialylated GBS. We propose that this neonatal immaturity might allow persistent GBS lung infection in some newborns, significantly increasing the risk of systemic spread to produce bacteremia, sepsis, and meningitis.

Multiple immune cell populations within the lung respond to serious bacterial infection and likely contribute to the subsequent repair process. Developmental immaturity of these cell populations therefore contributes to infectious disease risk and pathogenesis in newborns. Our data reinforce the paradigm of incomplete lung myeloid cell differentiation at birth with identification of key contributing lectin-glycan interactions and associated receptor signaling pathways. Sn-expressing NAMϕ populations were present at low numbers in juvenile mice and not detected in newborns. Different populations of IMϕ and DC were also

difficult to identify in newborn mouse lungs, potentially owing to their incomplete differentiation. Although we conclude that neonatal GBS susceptibility is significantly impacted by AMϕ immaturity, additional immune development defects also make the newborn particularly vulnerable.

THP is the predominant protein found in the urine, with diverse functions ranging from homeostasis to immune regulation and urinary tract defense (79). As much as 40% of the mass of THP is due to its glycosylation, including the terminal sialic acids (79). Many of its immune regulation functions involved neutrophils and renal interstitial macrophages. $THP^{-/-}$ mice had fewer renal interstitial macrophages and reduced phagocytosis, though had neutrophilia stemming from increased granulopoiesis in the bone marrow (80). This increased granulopoietic activity was largely due to increased IL-23 and IL-17 signaling (80). THP bound to Siglec-E on murine neutrophils and Siglec-9 on human neutrophils and reduced reactive oxygen species production and killing (74). Though despite inhibiting neutrophil killing, $THP^{-/-}$ mice were more susceptible to uropathogenic *E. coli* infections largely due to the role of THP in blocking bacterial adhesion and preventing overactive immune responses (74). In addition to its cellular regulation, THP can also act as a 'sponge' blocking effects of secreted cytokines and other inflammatory mediators, showing binding affinity for IL-1β, IL-2, TNF-α, and complement C1q (81-84). THP is capable of dampening inflammation at several different levels, thus the effects that we saw in the $THP^{-/-}$ neonates may not necessarily be a result of THP Sia-Siglec-E interactions on fetal pre- AMϕ. Therefore, we cannot discount secondary effects on fetal pre- AMϕ.

The discovery of Sn as being a critical receptor for the recognition of GBS created a unique translational aspect of this dissertation. We identified the absence of Sn expression on

neonatal AMϕ as being the underlying mechanism of neonatal susceptibility to GBS infection. If we could increase Sn expression on neonatal AMϕ, then we may be able to 'close' the window of susceptibility prior to exposure at birth and prevent severe disease. Increases in Sn expression have been reported prior in the literature, most often with the interferons, IFN-γ and IFN-α (67, 68). Online database searches for transcriptional regulators of the *Siglec1* gene yielded NF-κB p65, STAT1, STAT6, IRF1, and PPAR-γ as possible regulators of Sn (65, 66). However, IFN-γ and IFN-α both failed to increase Sn *in vivo* and had deleterious off target effects, including neutrophilia after IFN-γ, and stillbirth. Rosiglitazone, a PPAR-γ agonist, only increased Siglec-F expression after *in vivo* treatment, perhaps indicating accelerated AMϕ maturation as PPAR-γ is a critical factor for AMϕ maturation (45, 46). Chromatin accessibility could be playing a role in the inability of IFNs to upregulate *Siglec1* expression. The ATAC-seq data did reveal 1 site that was differentially more accessible in the adult compared to the PND4 neonate. Analysis of this differentially accessible site on ConTra did reveal putative STAT6 binding sites, though STAT6 binding sites were also found throughout the promoter and UTRs. By flow cytometry, the cell surface expression of Sn gradually increased from PND1 to adulthood, with PND0 neonatal pre-AMϕ not expressing Sn. Therefore, it is possible that the *Siglec1* gene is being silenced by inaccessible chromatin at birth, and the maturational process of AMϕ results in chromatin remodeling and the 'opening' of the promoter regions of *Siglec1* for transcription. ATAC-seq data from PND0 or PND1 neonatal pre-AMϕ could then reveal whether the *Siglec1* gene is more 'closed off' than the PND4 neonates, revealing possible chromatin remodeling. There could also be a developmental delay in JAK/STAT signaling pathway activity where the relative deficiency

in neonatal STAT signaling results in decreased expression of STAT regulated genes. We were thus unable to test whether increased Sn expression on neonatal AMϕ would be protective against GBS infection in our mouse model and could not evaluate the therapeutic potential of increased Sn expression in GBS infections.

In this dissertation we developed a novel intranasal model of GBS infection and show conclusively that neonatal susceptibility to GBS pneumonia derives from an inability of neonatal AMϕ to recognize the outer capsule of GBS. GBS exploits neonatal AMϕ, expressing only the inhibitory Siglec-E at birth, to dampen host immunity and escape killing creating a window of susceptibility to severe disease. This window closes upon maturation of the immature neonatal AMϕ and the subsequent expression of the phagocytic Siglec receptor, Sialoadhesin. Expression of Sialoadhesin allows macrophages to phagocytose the encapsulated GBS and prevent persistent infection and limit tissue damage. Importantly, this intranasal model of GBS infection allowed us to compare the immune responses to GBS across several different developmental stages as the inoculum of GBS could be adjusted based on weight to normalize for differences in body mass. The gaps in knowledge of neonatal susceptibility to GBS could have been due to a lack of comparative studies between adult and neonatal immune responses to GBS infection and difficulty in studying PND1 neonatal mice. This intranasal model can be adapted to study other such important neonatal pathogens to understand possible mechanisms of susceptibility in neonates that are not present in adults. This dissertation also revealed very important differences in the neonatal immune response to GBS infection. Even just 1 day apart between infection led to dramatic differences in recovered CFU and survival profiles. These findings underscore the importance of clear

definition of the day of life in neonates at the time of infection and in testing many different stages during the 'neonatal' period in any infection study.

The immunosuppression and negative regulation of Sn created by Siglec-E ligation by Sia revealed an intriguing possibility for AMϕ development. While unable to detect either the α2-3 or α2-6 sialic acid linkages in the fetal lung, we did detect the sialylated THP in the lung. We propose then that THP enters the lungs via aspiration of amniotic fluid, of which urine is a major component at the end of gestation. This proposed mechanism of a urinary protein influencing lung macrophage development is unique and provides another novel layer of fetal immune regulation. Ingestion of amniotic fluid, and thus THP, would then also provide a soluble systemic source of sialic acid capable of systemic suppression of the developing fetal immune system. Suppression of the fetal immune system could limit potentially damaging inflammation and preserve organ development. This lab has shown previously that NF-kB activation inhibits lung airway branching and leads to neonatal demise due to underdeveloped lungs (85). Future experiments should define Siglec-E expression across many key fetal tissues and immune cells to determine where in the developing fetus THP could be regulating immune cell development. RNA sequencing on fetal pre-AMϕ and other immune cells from both THP WT and KO neonates would reveal transcriptional changes that occur as a result of THP-Siglec-E interactions. Lung histology should also be compared between THP WT and KO neonates to determine whether the loss of this potentially important brake affects lung development, as constitutively active NF-κB inhibits lung development and leads to neonatal mortality. Infection of THP WT and KO neonates could show whether a potentially more pro-inflammatory state during fetal development leads to better protection from pathogens after birth.

APPENDIX: FIGURES AND TABLES

Figure 1. Increased Mortality and Persistence of Lung Injury in Neonatal GBS Infection
(A) Kaplan-Meier survival curve showing increased mortality in neonatal mice infected with intranasal GBS. All mice were given 28,000 CFU/g body weight of GBS. Neonatal mice (red) were infected within 24 h of delivery, juvenile mice (blue) were infected on day 7 of life, adult mice (black) were 6–8 weeks of age at infection. GBS-infected animals are shown with solid lines. Controls (dashed lines) were given identical anesthesia but intranasal sterile saline. ***$p < 0.005$ using the Mantel-Cox test ($n = 15–29$).
(B) CFU recovered from lung 1, 3, and 7 days after infection from adults, juvenile, and neonatal mice. Data are represented as mean ±SEM. *$p < 0.05$, **$p < 0.01$ using Mann-Whitney U test ($n = 6–9$).
(C) Representative H&E-stained sections obtained from mouse lungs 1, 3, and 7 days after GBS infection demonstrates initial lung injury and inflammation in all mice, with differential resolution by day 7. Scale bar, 100 mm.
(D) Neonatal mice displayed persistence of lung pathology following GBS infection. Lung pathology scoring was performed by three independent, blinded reviewers. Each experimental group included four to six animals with three representative images taken in a systematic method from each animal for a total of 12–18 images per group. The box is bound by the 25th and 75th percentile; the middle line represents the median value. The whiskers represent the minimum and maximum values. *$p < 0.05$, **$p < 0.01$, ***$p < 0.005$, ****$p < 0.001$ using one-way ANOVA.

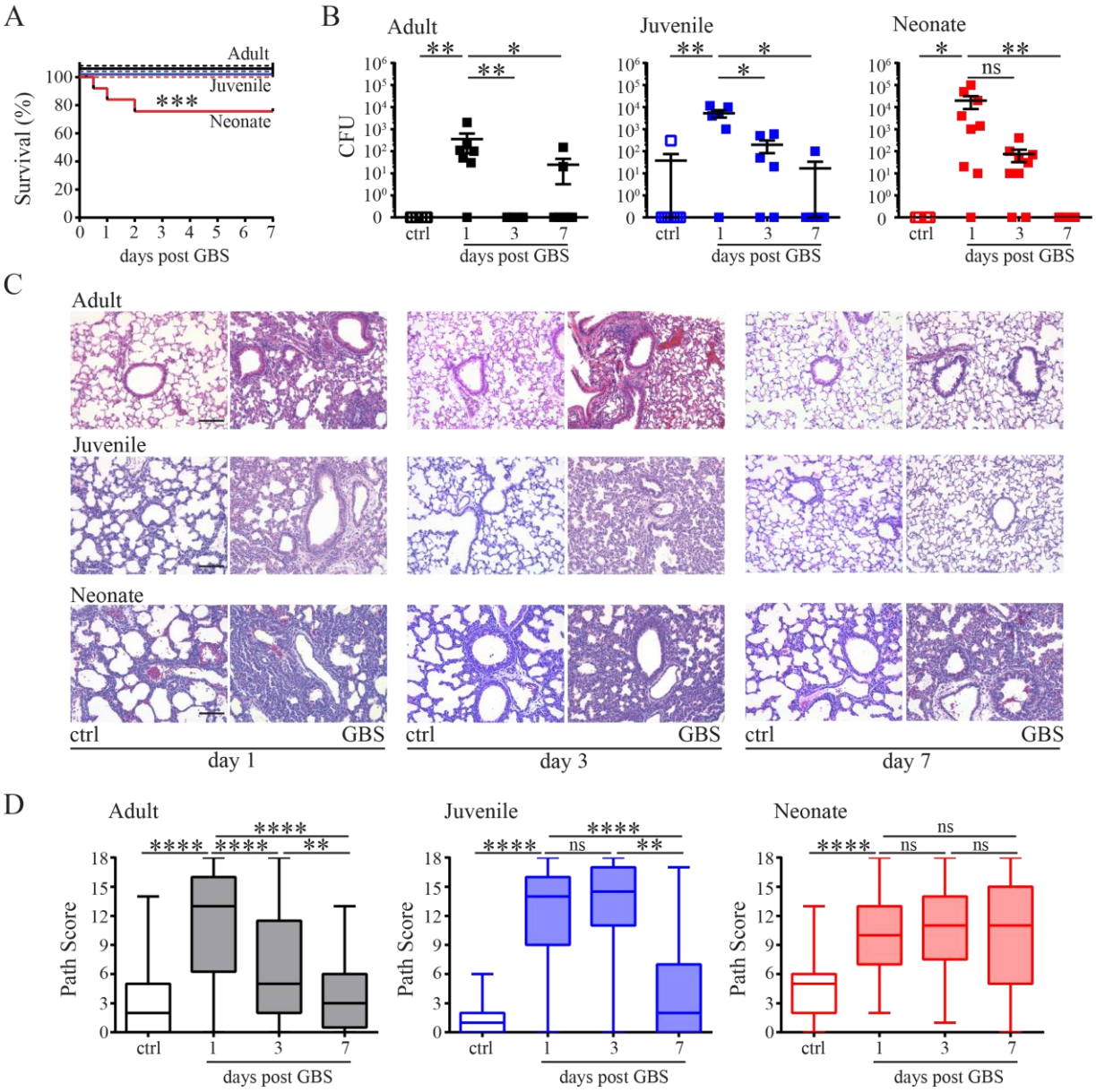

Figure 1. Increased Mortality and Persistence of Lung Injury in Neonatal GBS Infection

Figure 2. Delayed Kinetics of Lung Inflammation and GBS Clearance by Alveolar Macrophages in Neonatal GBS Pneumonia

(A) In adult mice, GBS infection induced inflammatory mediator expression in lung tissue between 2 and 6 h post infection. mRNA expression measured by real-time PCR and represented as fold change compared with control animals using Gapdh for normalization. Levels of *Il1b*, *Il6*, and *Cxcl1* all fell to baseline values by 24 h. Data are represented as mean ±SEM. Significance calculated using DCT values. *$p < 0.05$, **$p < 0.01$, ****$p < 0.001$ using unpaired t test. (n =5–8 mice per time point).

(B) In contrast to adult mice, increased expression of *Il1b*, *Il6*, and *Cxcl1* in neonatal mice was not detected until 24 h after GBS infection. Significance calculated using DCT values. *$p < 0.05$, **$p < 0.01$ using unpaired t test. (n = 4–6 mice per time point).

(C) Differential accumulation of $CD68^+$ inflammatory cells in the lungs of adult mice following GBS infection compared with neonates. Confocal immunofluorescence micrographs showed accumulation of $CD68^+$ cells (green) within 12–24 h after GBS infection in adults. Neonatal lungs did not display similar cellular accumulation. Images representative of two to three separate experiments. Cell nuclei stained with DRAQ5 (blue). Scale bar, 100 mm.

(D) Lack of GBS clearance in neonatal mouse lungs. GBS CFU recovered from the lungs of adult, juvenile, and neonatal mice were measured 0.5, 2, 6, 12, and 24 h after infection. Data are represented as mean ±SEM. *$p < 0.05$, **$p < 0.01$, ***$p < 0.005$ using Mann-Whitney U test (n = 6–9).

(E) Susceptibility to GBS infection was unique to newborn mice. Left panel shows Kaplan-Meier survival curve from neonatal mice infected with GBS ($2.8x10^6$ CFU/g body weight) on postnatal day 1 (red), postnatal day 2 (blue), and postnatal day 3 (black). *$p < 0.05$ using the Mantel-Cox test (n = 10–17). Right panel shows GBS CFU recovered from lung and spleen from surviving animals 21 days after infection. Systemic persistence of infection was primarily detected in mice infected on P1. Data are represented as mean ±SEM.

(F) Uptake of GBS by $CD68^+$ lung macrophages. Confocal immunofluorescent micrographs show localization of GBS (red) within $CD68^+$ cells (green) soon after infection in adult and juvenile mouse lungs. However, in neonatal lungs, GBS uptake by $CD68^+$ cells was minimal. Insets on the right show higher magnification of regions outlined in 24-h images. Nuclei stained with DRAQ5 (blue). Images representative of two to three independent experiments. Scale bar, 25 mm.

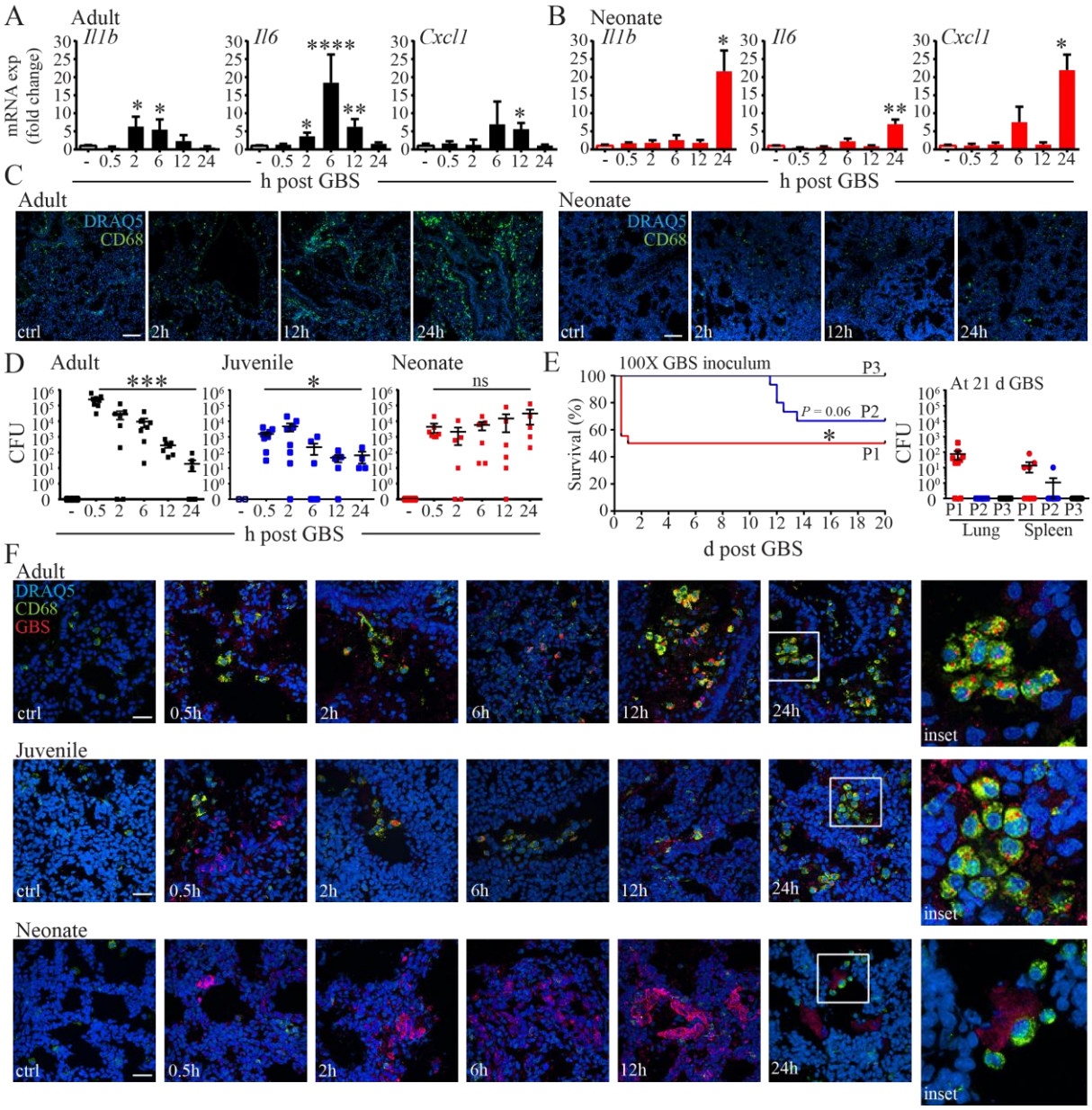

Figure 2. Delayed Kinetics of Lung Inflammation and GBS Clearance by Alveolar Macrophages in Neonatal GBS Pneumonia

Figure 3. Mature AMϕ Are Required for Rapid GBS Clearance

(A) Flow cytometry of CD11b expression in $CD45^+$ $CD64^+$ $F4/80^+$ lung macrophages from adult, juvenile, and neonatal mice following GBS infection. In adult mice, GBS increased CD11b expression in Siglec-F^+ AMϕs within the first 3 days following infection. Juvenile mice had increased CD11b expression on day 3. However, neonatal lung macrophages did not increase CD11b following GBS infection compared with control, uninfected mice. Data representative of three to four independent experimental replicates.

(B–D) AMϕ depletion using liposomal clodronate reduces GBS killing in adult lungs.

(B) Flow cytometry confirming depletion of AMϕs using intranasal liposomal clodronate compared with control mice given empty liposomes. Data representative of two independent experimental replicates.

(C) Confocal immunofluorescent micrographs showed GBS persistence (red) in adult mice 24 h after infection (and 72 h after clodronate treatment). Majority of larger $CD68^+$ cells (green) are depleted following liposomal clodronate. Smaller cells expressing lower levels of CD68 likely represent recruited monocytes with reduced capacity to phagocytose GBS. Nuclei counter stained with DRAQ5 (blue). Images taken 24 h after infection Scale bar, 25 mm.

(D) Depletion of AMϕs from adult mice reduced GBS killing. CFU recovered from lung 24 h after infection from adults given intranasal clodronate or empty liposomes 48 h prior to infection. Data are represented as mean ±SEM. $^{**}p < 0.01$ using Mann-Whitney U test (n = 8).

(E and F) Defective GBS killing in neonatal $Csf2^{-/-}$ mice.

(E) Confocal immunofluorescent micrographs show scattered GBS (red) in $Csf2^{-/-}$ mouse lungs 24 h after infection. Scale bar, 25 mm.

(F) Neonatal $Csf2^{-/-}$ mice had reduced GBS killing 24 h after infection. Data are represented as mean ±SEM. $^{*}p < 0.05$ using Mann-Whitney U test (n = 5–10).

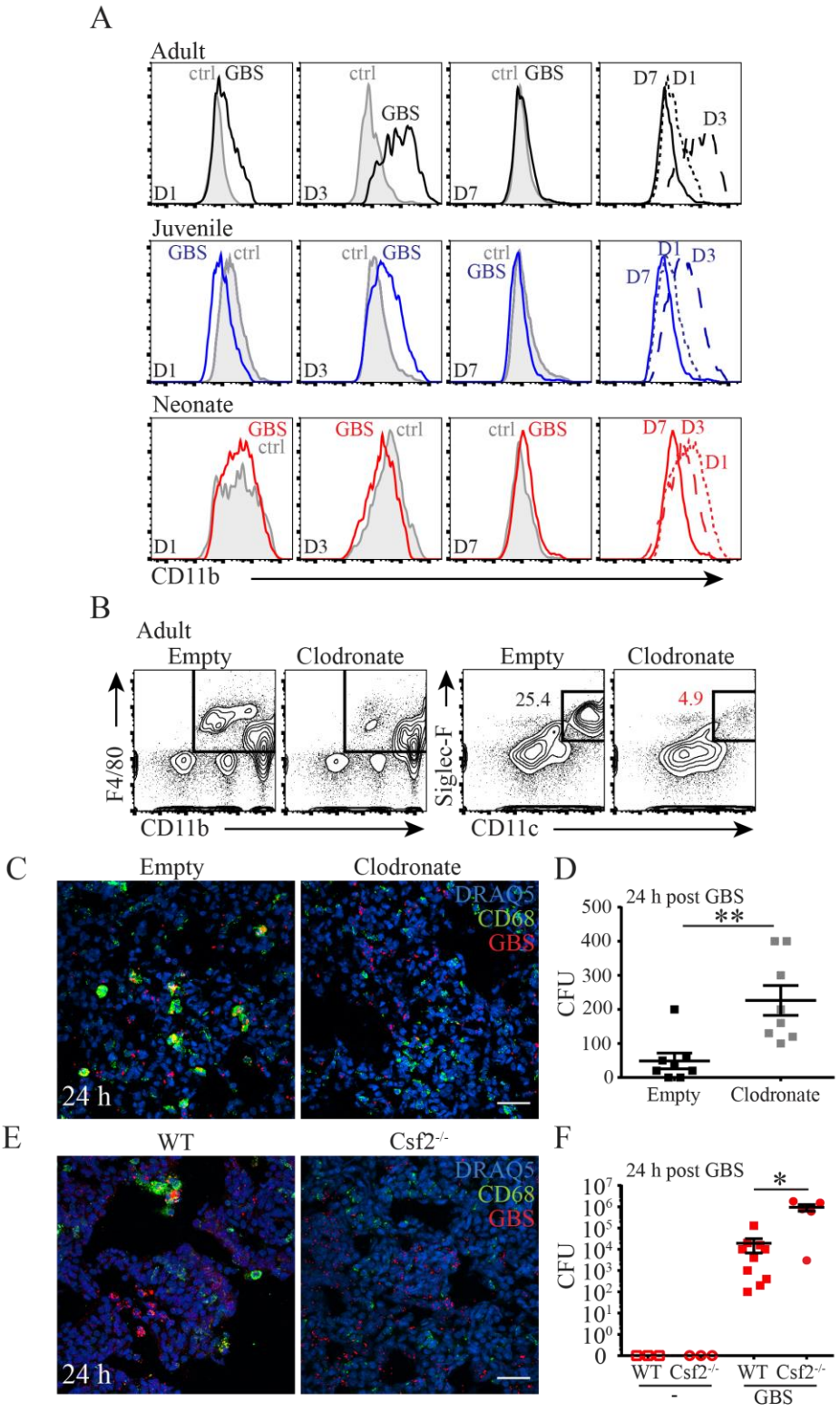

Figure 3. Mature AMϕ Are Required for Rapid GBS Clearance

Figure 4. Developmental Maturation of Lung Myeloid Siglec Expression

(A–C) Flow cytometry analysis of Sn and Siglec-E in lung myeloid populations.

(A) Gating strategy for $CD45^+$ cells from adult lungs. $F4/80^{hi}$ $CD11b^{lo}$ cells gated on Siglec-F and CD11c to identify AMϕ (Siglec-F^+ $CD11c^+$) and NAMϕ ($CD11c^{lo}$). Neutrophils (PMN) identified as $F4/80^-$ $CD11b^+$ $CD64^-$. The $CD11b^+$ $F4/80^{lo}$ population was then gated on Siglec-F and CD11c to identify $CD11b^+$ AMϕ, the $CD11c^+$ Siglec-F^- population of interstitial macrophages/monocytes and dendritic cells (IMϕ/DC) and $CD11c^-$ Siglec-F^- interstitial macrophages/monocytes (IMϕ). Expression of Sn and Siglec-E are shown below for each myeloid population.

(B) Gating strategy for juvenile lungs similar to parameters used for adults.

(C) For neonatal lungs, PMNs are identified as $CD11b^+$ $F4/80^-$ Ly-$6G^+$. Total $F4/80^+$ population then gated on $CD64^+$ Ly-$6G^-$ cells, followed by Siglec-F and CD11c to identify Siglec-F^- $CD11c^-$ IMϕ and $CD11c^+$ AMϕ, including immature and developing AMϕ populations.

(D and E) Developmental changes in Sn and Siglec-E expression in lung immune cells as measured by flow cytometry. Sn and Siglec-E expression plotted for entire $CD45^+$ lung populations from adult, juvenile, and neonatal mice.

(F and G) Developmental changes in Sn and Siglec-E within lung macrophages. Sn and Siglec-E expression measured by flow cytometry and plotted for $CD45^+$ $F4/80^+$ $CD11b^+$ total macrophage populations from adult, juvenile, and neonatal mice. Gray shaded peak is the isotype control for each sample. Right panels show Median Fluorescent Intensity of Sn and Siglec-E in total macrophage populations. Data are represented as mean ±SEM. ***$p < 0.001$ using Mann-Whitney U test ($n = 3–8$).

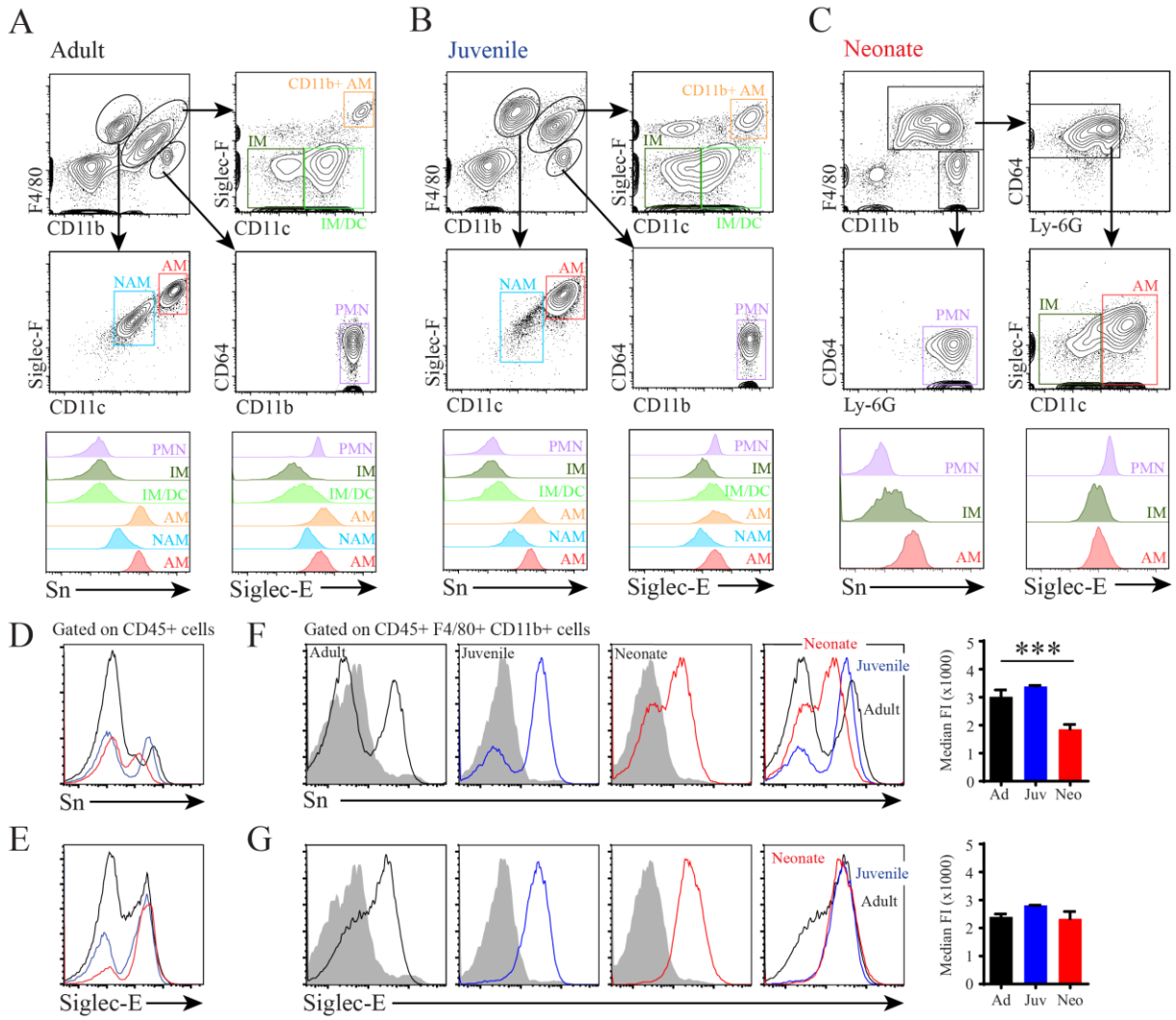

Figure 4. Developmental Maturation of Lung Myeloid Siglec Expression

Figure 5. Developmental Immaturity of AMϕ Siglec-Sialic Acid Detection Contributes to Neonatal GBS Susceptibility

(A) Neonatal lungs had reduced *Siglec1* mRNA expression compared with adults but similar levels of *Siglece*. Normalized to Gapdh and represented as fold change compared with adult samples. Data are represented as mean ±SEM. Significance calculated using DCT values. * = $p < 0.05$, using unpaired t test. (n = 4–6 mice per time point).

(B) Confocal immunofluorescent micrographs showing extensive Sialoadhesin expression (red) in adult $CD68^+$ macrophages following GBS infection (left panel). Presence of Sialoadhesin-expressing cells was reduced in neonatal lungs (right panel). Images taken 24 h after infection.

(C) Human *SIGLEC1* and *SIGLEC9* (human *Siglece* paralog) gene expression in lung macrophages obtained from human preterm newborns on day 1 and day 7 of life showing reduced *SIGLEC1* expression at birth with increased levels by 1 week of age. SIGLEC9 expression was unchanged. Expression measured by Affymetrix GeneChip Human Transcriptome 2.0 arrays. Boxplots are shown with mean as circle with arrows representing ±SD, median as white line with 95% confidence intervals as colored lines (n = 83 on day 1, n = 46 on day 7).

(D and E) Siglec-E is not required for GBS killing in adult mice.

(D) Similar CFU recovered from WT and SigE-/- adult mouse lungs 24 h after GBS infection (n = 11–15). Data are represented as mean ±SEM.

(E) Confocal immunofluorescent micrographs showed similar patterns of CD68 (green) and GBS (red) in WT and SigE-/- adult lungs 24 h after infection. Images are representative of three independent experimental replicates. Scale bar, 25 mm.

(F and G) GBS killing is increased in neonatal SigE-/- mice.

(F) Compared with WT controls, neonatal SigE-/- mice had reduced CFU recovered from lung 24 h after GBS infection. Data are represented as mean ±SEM. **$p < 0.005$ using Mann-Whitney U test (n = 10 for WT, n = 24 for SigE-/-).

(G) Confocal immunofluorescent micrographs demonstrated reduced GBS overall (red) and increased GBS phagocytosis by $CD68^+$ cells in SigE-/- neonatal mouse lungs 24 h after infection. Images are representative of three independent experimental replicates. Scale bar, 25 mm.

(H) Flow cytometry showing reduced Sialoadhesin expression in both adult and neonatal lung macrophages from $Csf2^{-/-}$ mice. Data are representative of two independent experimental replicates.

(I) Siglec-E expression in AMϕ was reduced in adult $Csf2^{-/-}$ mice compared with WT controls (left panel) but similar in neonatal $Csf2^{-/-}$ lung macrophages
(right panel). Data are representative of two independent experimental replicates.

(J) Killing of WT, ΔneuA, or ΔcpsD GBS was similar in adult mice 24 h after intranasal infection (n = 7–10). Data are represented as mean ±SEM.

(K) Confocal immunofluorescent micrographs showed only rare GBS staining (red) in adult mice 24 h after infection with either WT GBS or ΔneuA GBS. Images are representative of two to three independent experimental replicates. Scale bar, 25 mm.

(L) Neonatal mice had increased ability to kill GBS with defects in sialic acid capsule synthesis. CFU measured 24 h after infection. Data are represented as mean ±SEM. **$p < 0.01$ using Mann-Whitney U test (n = 7–10).

(M) Confocal immunofluorescent micrographs showed increased ΔneuA GBS (red) phagocytosis by $CD68^+$ macrophages (green) 24 h after infection. Images are representative of two to three independent experimental replicates.

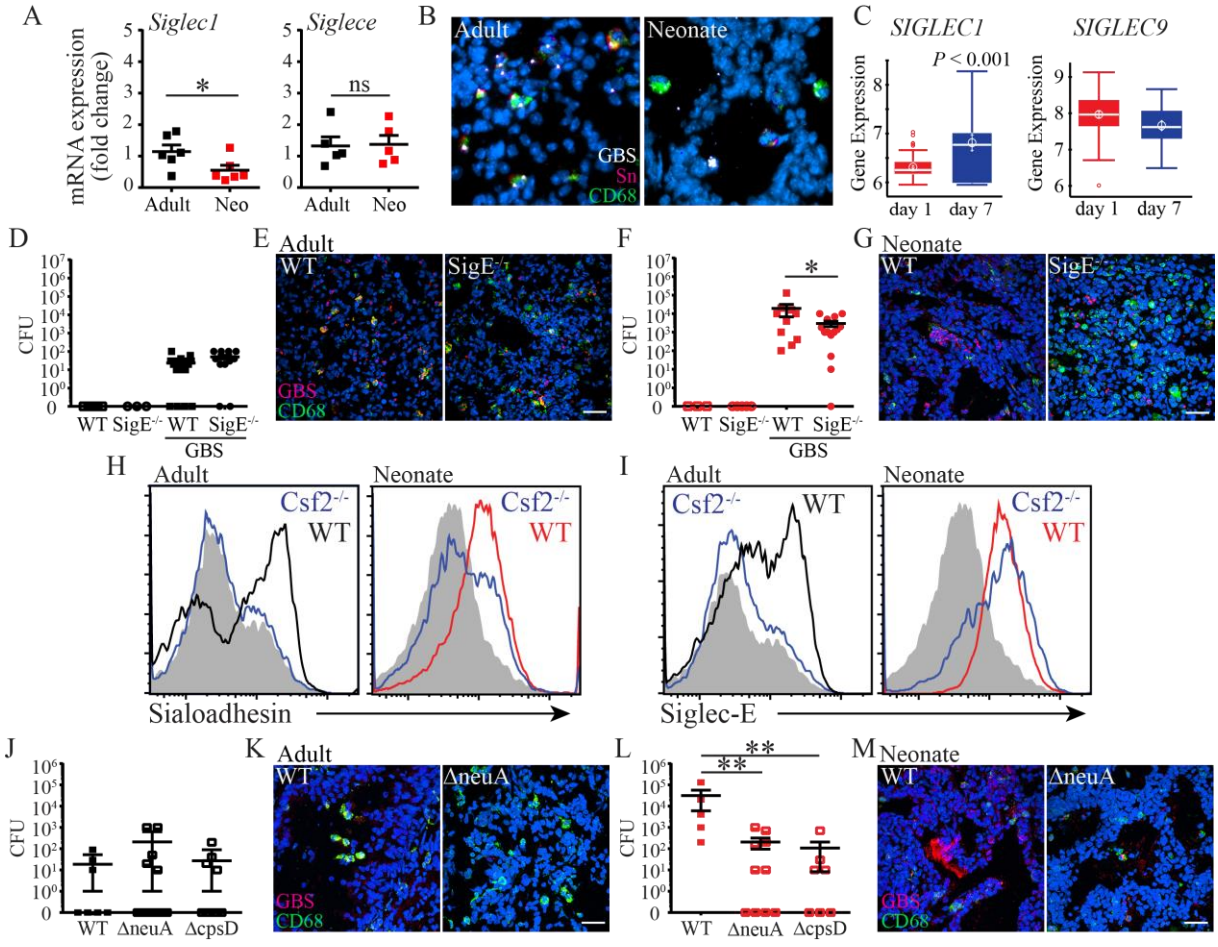

Figure 5. Developmental Immaturity of AMϕ Siglec-Sialic Acid Detection Contributes to Neonatal GBS Susceptibility

Figure 6. Sn Expression Declines Over Time Following GBS Infection
(A-F) Whole lung RNA obtained from control or infected mice 0.5, 2, 6, 12, or 24 hours after GBS.
(A) Adult and (B) Neonatal *Siglec1* mRNA expression measured by real-time PCR and represented as fold change compared with control animals using Gapdh for normalization. Expression decreases at 6 and 12 hours after infection in the adults and 0.5, 2, 6, and 12 h after infection in the neonates.
(C) Adult and (D) Neonatal *Siglece* mRNA expression measured by real-time PCR and represented as fold change compared with control animals using Gapdh for normalization. Expression unchanged in adults and neonates following infection.
(E) *Siglec1* expression compared between adults and neonates following GBS infection. Normalized to neonatal control sample. Adult expression is significantly higher than neonatal expression at 0.5 and 2 hours. Adult expression decreased relative to the neonatal samples at 6 and 12 hours, before slight recovery of expression at 24 hours.
(F) *Siglece* expression compared between adults and neonates following GBS infection. Normalized to neonatal control sample. Adult expression is significantly higher than neonatal expression at 0.5 and 2 hours. Adult expression decreased relative to the neonatal samples at 6 and 12 hours, before slight recovery of expression at 24 hours.

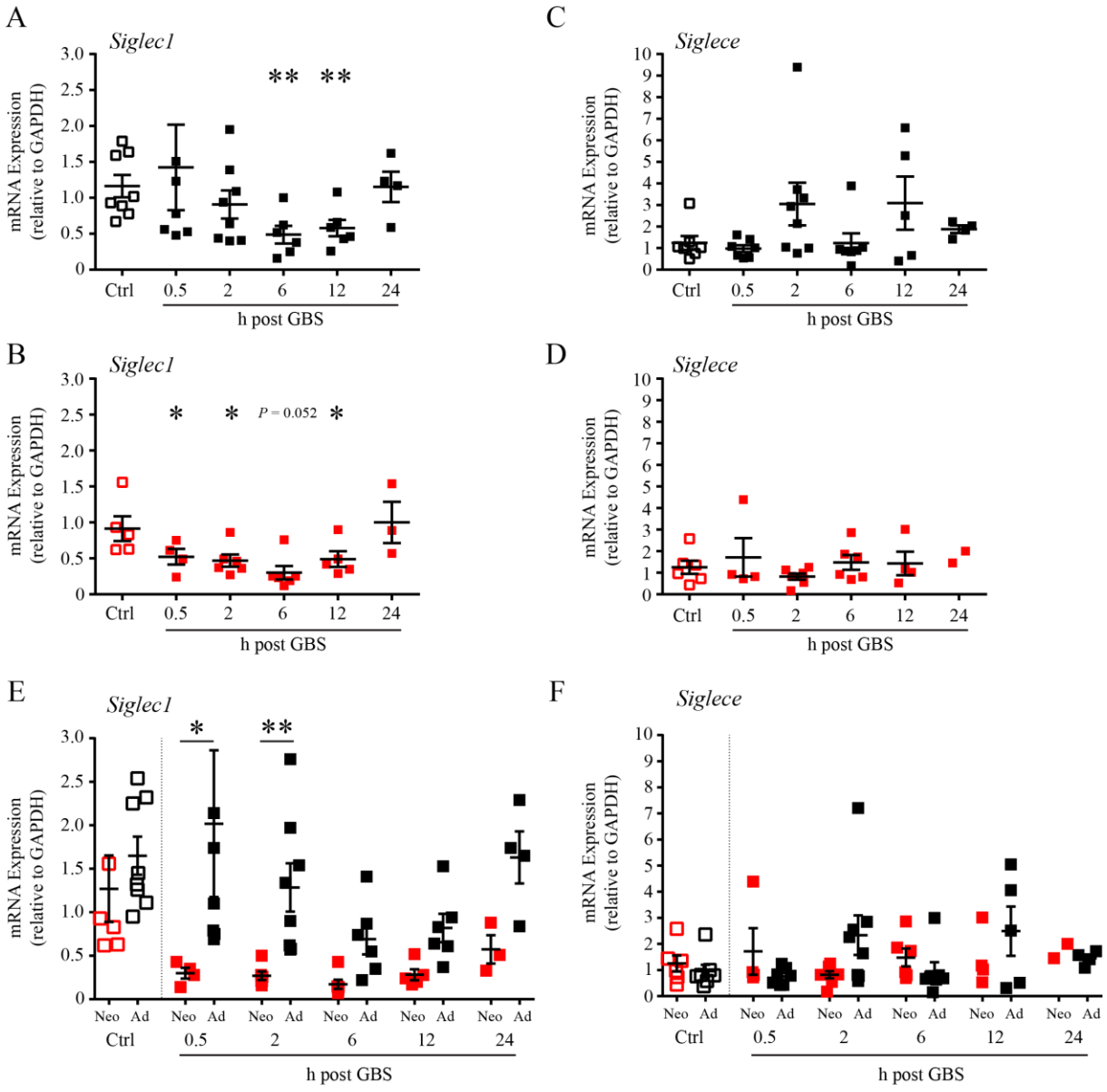

Figure 6. Sn Expression Declines Over Time Following GBS Infection

Figure 7. The Sia-Siglec-E Interaction Mediates Decreased Sn Expression Following Infection

(A) *Siglec1* mRNA expression in adults infected with either WT or ΔneuA GBS measured by real-time PCR and represented as fold change compared with uninfected control animals using Gapdh for normalization.

(B) *Siglec1* mRNA expression in neonates infected with either WT or ΔneuA GBS measured by real-time PCR and represented as fold change compared with control animals using Gapdh for normalization.

(C) *Siglece* mRNA expression in adults infected with either WT or ΔneuA GBS measured by real-time PCR and represented as fold change compared with control animals using Gapdh for normalization.

(D) *Siglece* mRNA expression in neonates infected with either WT or ΔneuA GBS measured by real-time PCR and represented as fold change compared with control animals using Gapdh for normalization.

(E) Sn cell surface receptor expression in Siglec-E WT and KO neonates. Expression measured by flow cytometry 24 h after infection or control saline treatment. Sn expression decreased 24 h after infection in the WT, remained stable in the Sig-$E^{-/-}$ neonates following infection.

(F) Siglec-E cell surface receptor expression in Siglec-E WT and KO neonates. Expression measured by flow cytometry 24 h after infection or control saline treatment. Siglec-E expression increased 24 h after infection in the WT.

(G-H) *Il1b* expression in adults infected with either WT or ΔneuA GBS (G) and neonates infected with either WT or ΔneuA GBS (H). Adults infected with ΔneuA GBS had significantly higher *Il1b* expression at 6 h, while neonates infected with ΔneuA GBS did not have increased expression at these timepoints.

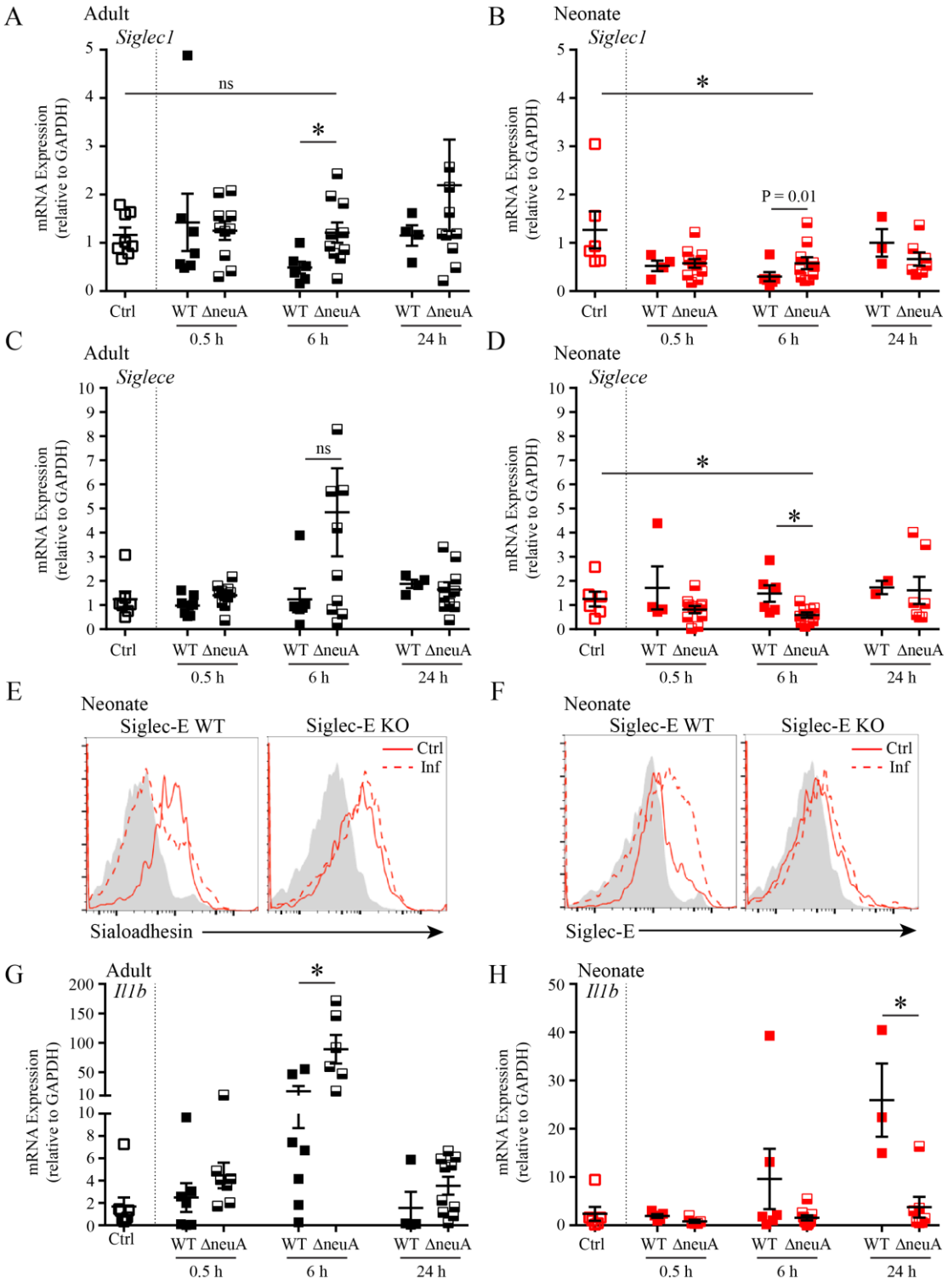

Figure 7. The Sia-Siglec-E Interaction Mediates Decreased Sn Expression Following Infection

Figure 8. *Siglec1* is Regulated by the STAT Pathway and is Differentially Accessible in the Adult

(A) Table showing the top results of *Siglec1* gene regulators from 3 different online databases: ChIPBase v2.0, ImmGen Enhancer Networks, and ConTra v3. Bolded factors indicate repeated hits across multiple databases

(B) Browser tracks from ConTra v3 depicting repeated putative STAT6 and C/EBPα binding sites in the *Siglec1* promoter and UTRs. STAT6 in light green, and C/EBPα in salmon.

(C) ATAC-seq data from Adults and PND4 neonates given intranasal PBS 2 h prior to cell sorting. RNA extracted from sorted AMϕ. Table shows 1 *Siglec1* site that is among the top 200 genes most differentially accessible in the adult compared to the PND4 neonate.

(D) Browser tracks from UCSC Genome Browser depicting the ATAC-seq data set. PBS or LPS treated adults and neonates showing the *Siglec1* (left) and *Siglece* (right) gene loci. Peaks represent the most accessible sites. The red box indicates the most differentially accessible site in (C).

A

Database	*Siglec1* Predicted TFBS	*Siglece* Predicted TFBS
ChIPBase v2.0	Spi1, Rela, C/EBPα, C/EBPβ, AhR, Egr2, PPAR-γ, **IRF1**, Ncor1, **STAT1**	Spi1, Rela, CEBP/α, CEBP/β, Erg, Meis1, Rfx6
ImmGen Enhancer Networks	E2f1, Bcl11b, Mef2c, Bcl, **IRF1**, **STAT6**	Elf1, Bcl, SpiB, Bcl11b, Maz, Nr2c1
ConTra v3	C/EBPα, **STAT6,** Mef2c	Bcl6, Spi1, SpiB, Meis1, CEBP/α

B

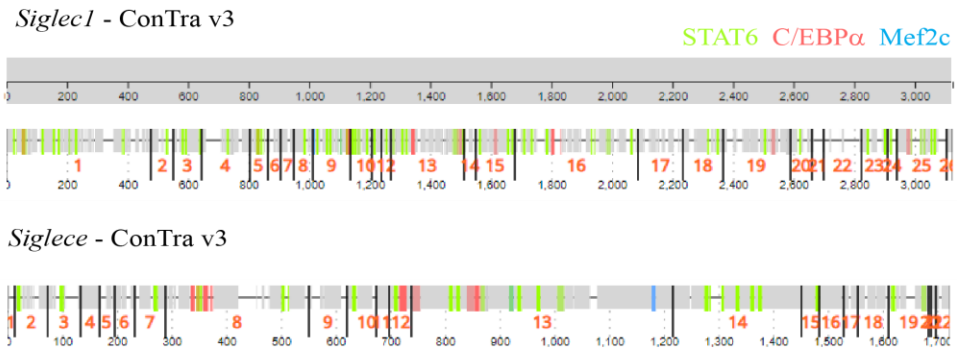

C

Most Differentially Accessible Sites - Adult PBS vs. P4 Neo PBS

Gene	Start	End	Distance to TSS	Peak Score	log FC	Adj P value
Siglec1	Chr 2 131106053	Chr 2 131106253	-19388	30.6	0.592	0.0121

D

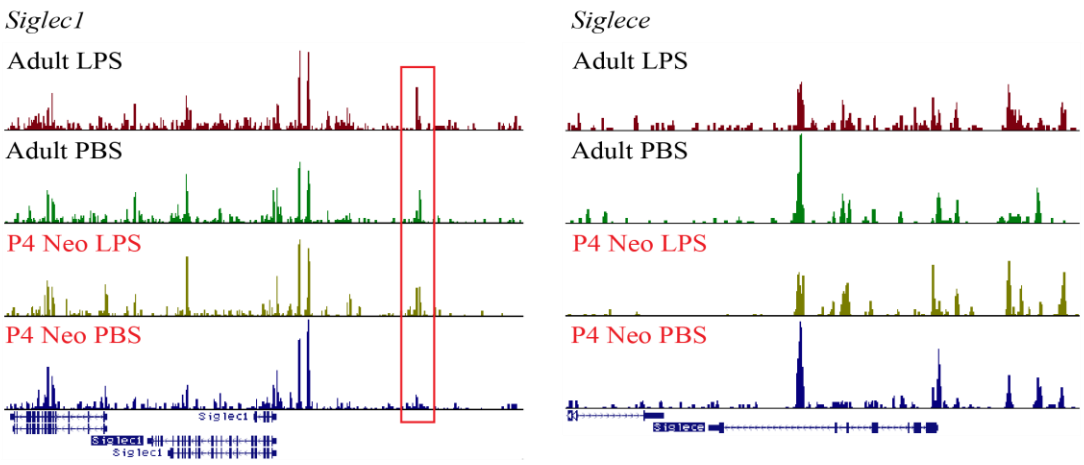

Figure 8. *Siglec1* is Regulated by the STAT Pathway and is Differentially Accessible in the Adult

Figure 9. RG, IFN-α,γ Did Not Increase Sn Expression on the First Day of Life
(A) PND2 neonatal whole lung cells were cultured for 8 (left), 14 (middle), or 38 (right) h in the presence of Pam3CSK4, TNF-α, GM-CSF, LPS, or IFN-γ. Sn Expression was measured by flow cytometry. Dashed line represents Sn expression of media control. Gated on $CD45^+$ $F4/80^+$ $CD11b^+$ macrophages.
(B) Diagram of the timeline used in *in vivo* Sn expression experiments. Pregnant mothers were given intraperitoneal (IP) injections of either IFN-a, IFN-g, RG (0.1 or 0.5 mg doses) or the corresponding vehicle control at E18. Neonatal Sn expression was measured by flow cytometry postnatally at PND0 or PND4.
(C) Sn (left) or Siglec-F (right) expression on PND0 neonatal macrophages after prenatal administration of IFN-α, IFN-γ, or the vehicle control. Gated on $CD45^+$ $F4/80^+$ $CD11b^+$ macrophages. Dashed line represents Sn expression of vehicle control.
(D) Sn (left) or Siglec-F (right) expression on PND0 neonatal macrophages after prenatal administration of 0.1 or 0.5 mg rosiglitazone (RG) or the vehicle control. Gated on $CD45^+$ $F4/80^+$ $CD11b^+$ macrophages. Dashed line represents Sn expression of vehicle control.
(E) Sn (left) or Siglec-F (right) expression on PND4 neonatal macrophages after prenatal administration of 0.1 or 0.5 mg rosiglitazone (RG) or the vehicle control.. Gated on $CD45^+$ $F4/80^+$ $CD11b^+$ macrophages. Dashed line represents Sn expression of vehicle control.
(F) CD11b x F4/80 flow cytometry plots depicting myeloid cell populations of PND0 neonatal macrophages after prenatal administration of IFN-α, IFN-γ, or the vehicle control. Gated on $CD45^+$ cells.
(G) CD11b x F4/80 flow cytometry plots depicting myeloid cell populations of PND0 neonatal macrophages after prenatal administration of 0.1 or 0.5 mg rosiglitazone (RG) or the vehicle control. Gated on $CD45^+$ cells.

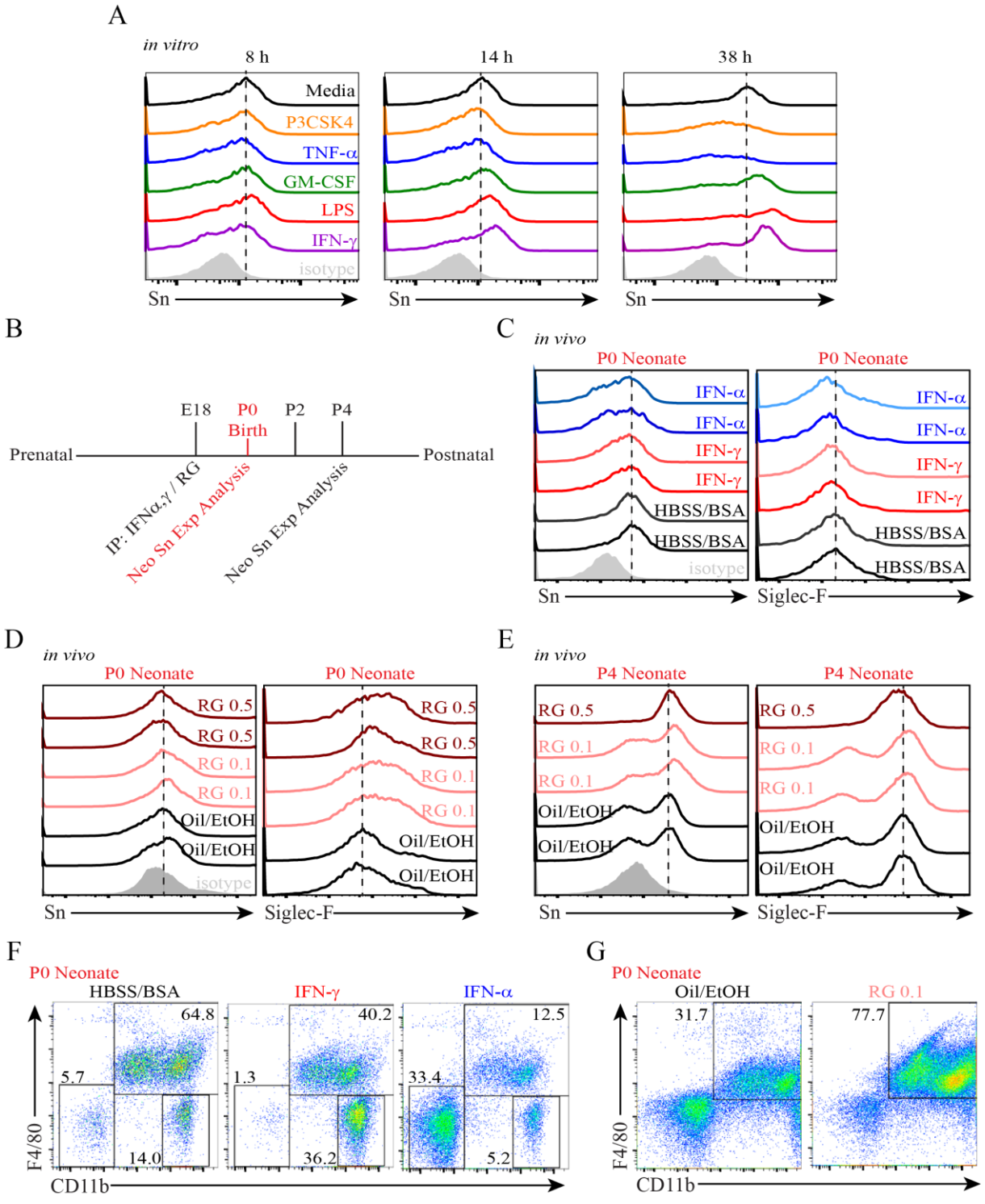

Figure 9. RG, IFN-α,γ Did Not Increase Sn Expression on the First Day of Life

Figure 10. Sialic Acid is Not Expressed in the Developing Fetal Lung
(A) Immunofluorescent micrographs at 10X magnification from E15, PND1, PND7, and adult lungs stained with α2-3 sialic acid (green) and CD68 (red). Counterstained with DRAQ5. α2-3 sialic acid staining was only apparent after birth.
(B) Immunofluorescent micrographs at 10X magnification from E15, PND1, PND7, and adult lungs stained with α2-6 sialic acid (green) and CD68 (red). Counterstained with DRAQ5. The mouse lung does not contain any α2-6 sialic acid.

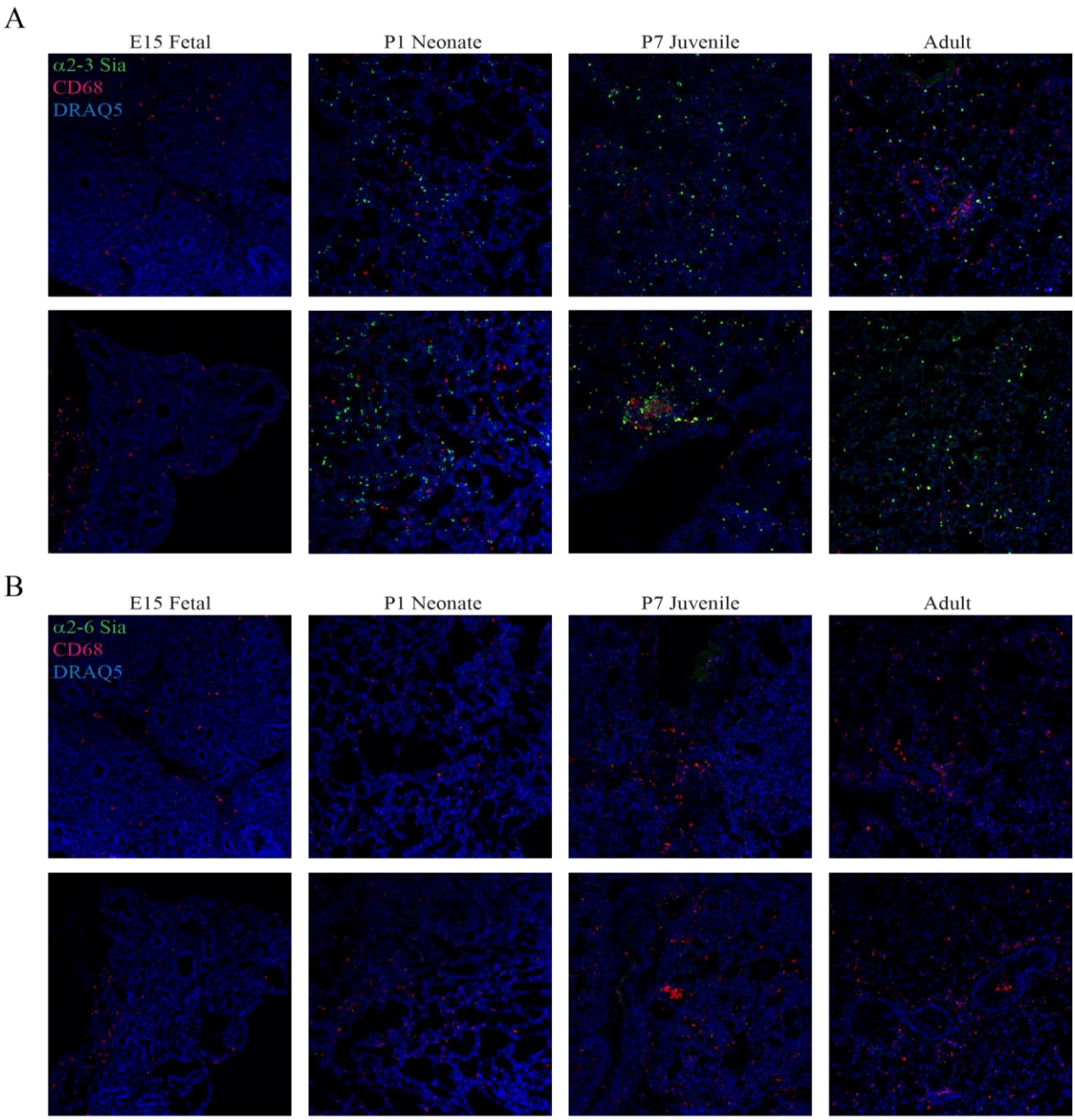

Figure 10. Sialic Acid is Not Expressed in the Developing Fetal Lung

Figure 11. Loss of THP Alters Neonatal Siglec-E and Siglec-F Receptor Expression
(A) Graphical hypothesis of sialylated THP and pre-AMϕ interactions via Siglec-E. Created using BioRender.
(B) Concentration (pg/mL) of THP in fetal amniotic fluid, lungs, and liver, and neonatal lungs. Dashed line represents limit of detection.
(C) Immunofluorescent micrographs at 10X magnification from E15, E18, PND7, and adult lungs stained with CD68 (green) and THP (red), Counterstained with DRAQ5
(D) Immunofluorescent micrographs at 40X magnification from E15 and adult lungs stained with CD68 (green) and THP (red), Counterstained with DRAQ5
(E) Flow cytometry analysis from P1, P2, and P8 lungs from WT and THP KO neonates. Top – Siglec-E vs. Siglec-F plot showing a subpopulation of Siglec-E^{lo} cells at P1 and P2, absent in P8. Bottom – Histogram plot of Siglec-E expression on $CD45^+$ $F4/80^+$ $CD11b^+$ cells showing the same subpopulation of Siglec-E^{lo} cells at P1.
(F) Median Fluorescent Intensities of Siglec-E, Siglec-F, and Sialoadhesin expression on $CD45^+$ $F4/80^+$ $CD11b^+$ cells. THP KO macrophages had significantly lower expression of Siglec-E at each timepoint compared to WT but increased Siglec-F expression at P2. Data are represented as mean ±SEM. *$p < 0.05$ using Mann-Whitney U test ($n = 4$-8).

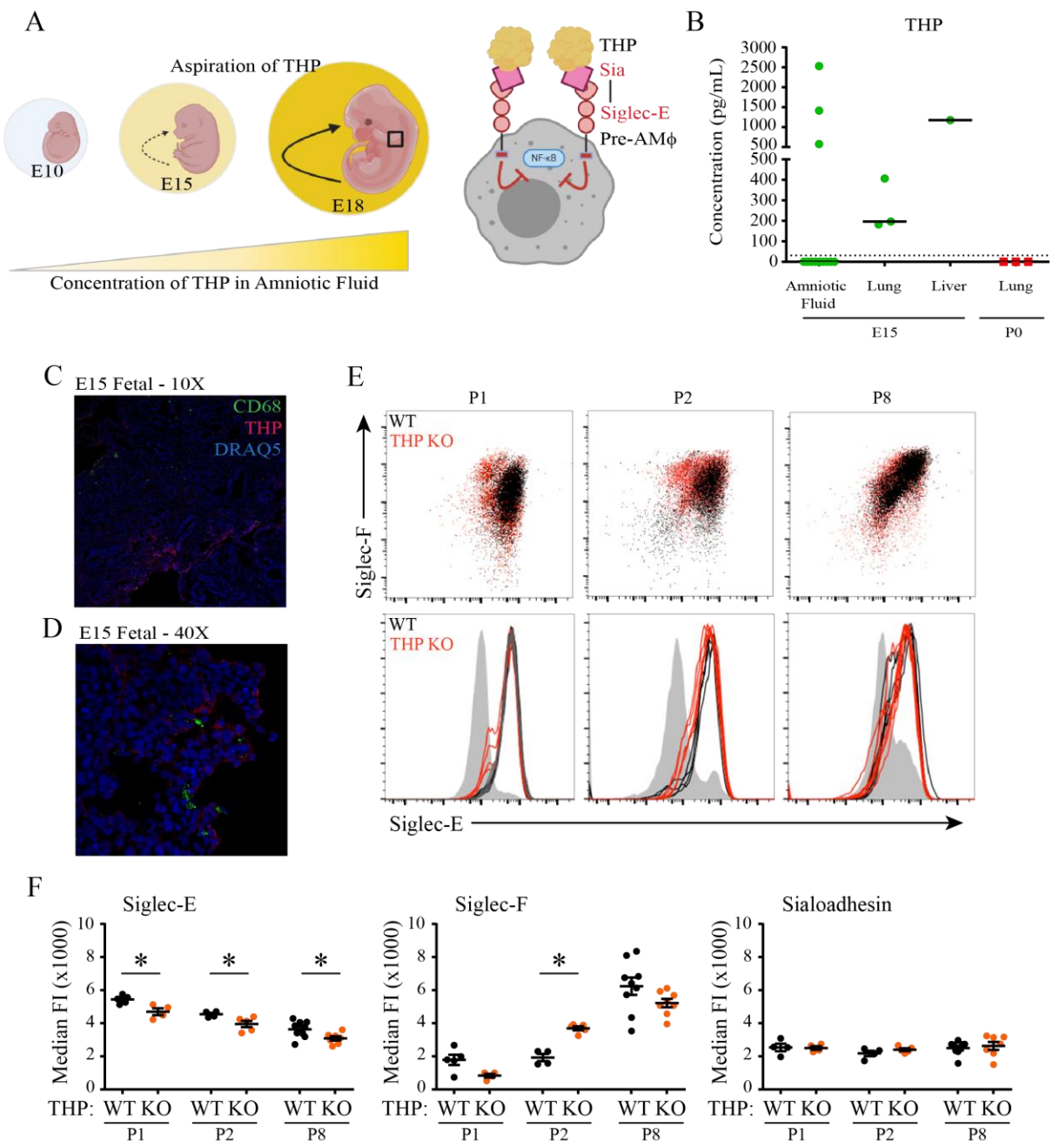

Figure 11. Loss of THP Alters Neonatal Siglec-E and Siglec-F Receptor Expression

Figure S1. Gating strategy for measuring Siglec receptor expression on lung macrophage populations.
(A-C) Gating strategy used for analyzing macrophages throughout the paper and Siglec receptor expression in Figure 4. $CD45^{+}$ $F4/80^{+}$ $CD11b^{+/-}$ macrophages were analyzed across all developmental timepoints. Importantly, Siglec-F expression occurs during the first week of postnatal life and is therefore absent in neonatal lung pre-alveolar macrophages.

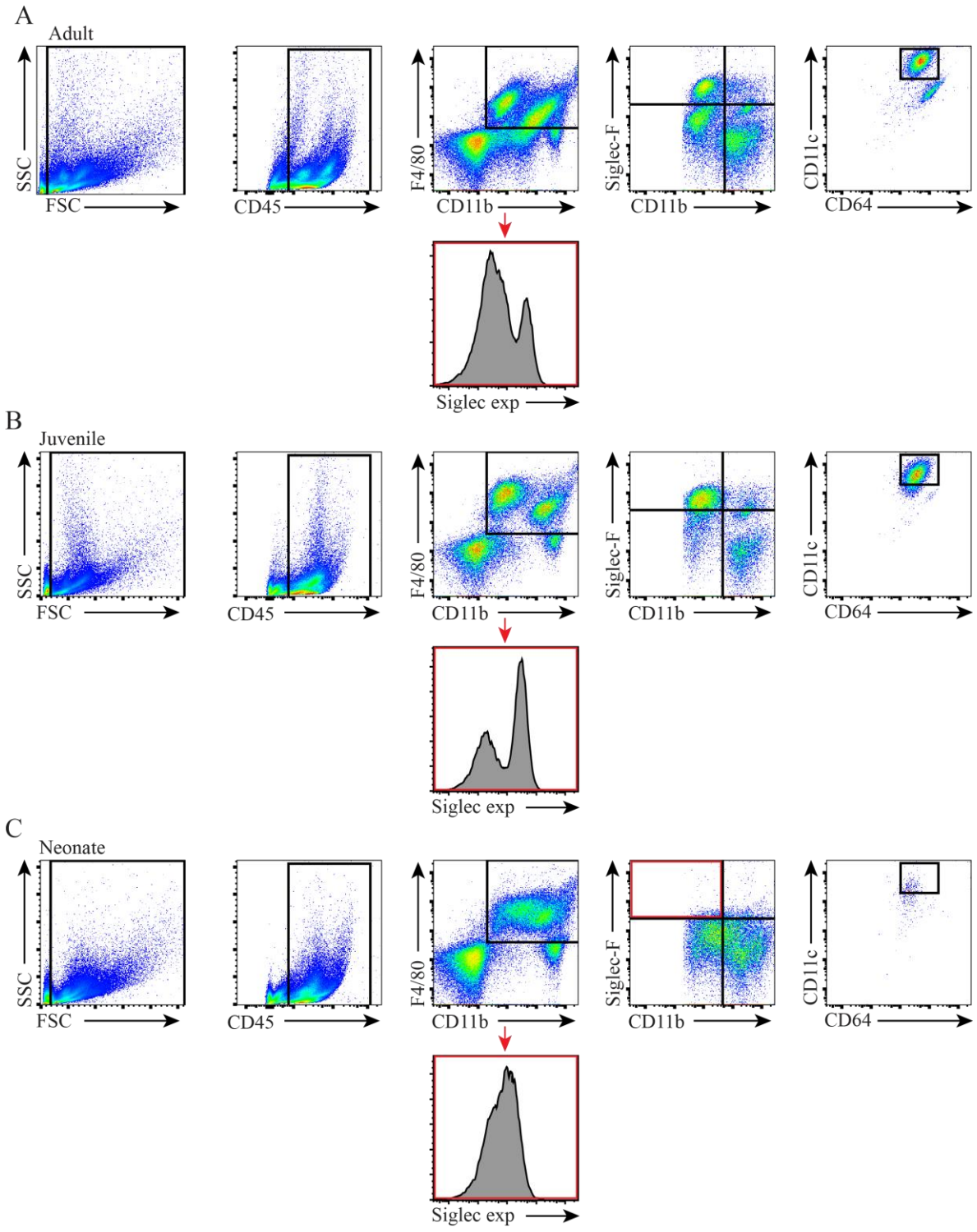

Figure S1 (Refers to Figure 4). Gating Strategy for Measuring Siglec Receptor Expression on Lung Macrophage Populations.

Figure S2 (Refers to Figure 3). Changes in macrophage marker expression following GBS infection.
FACS data showed increased CD11b expression in adult AMϕ following GBS infection with resolution by day 7. Juvenile mice showed similar if less obvious increase in CD11b expression. In contrast, neonatal lung macrophages continued the normal developmental transition to express Siglec-F following GBS infection without any measurable changes in CD11b expression. Arrows represent changes in population relative to control.

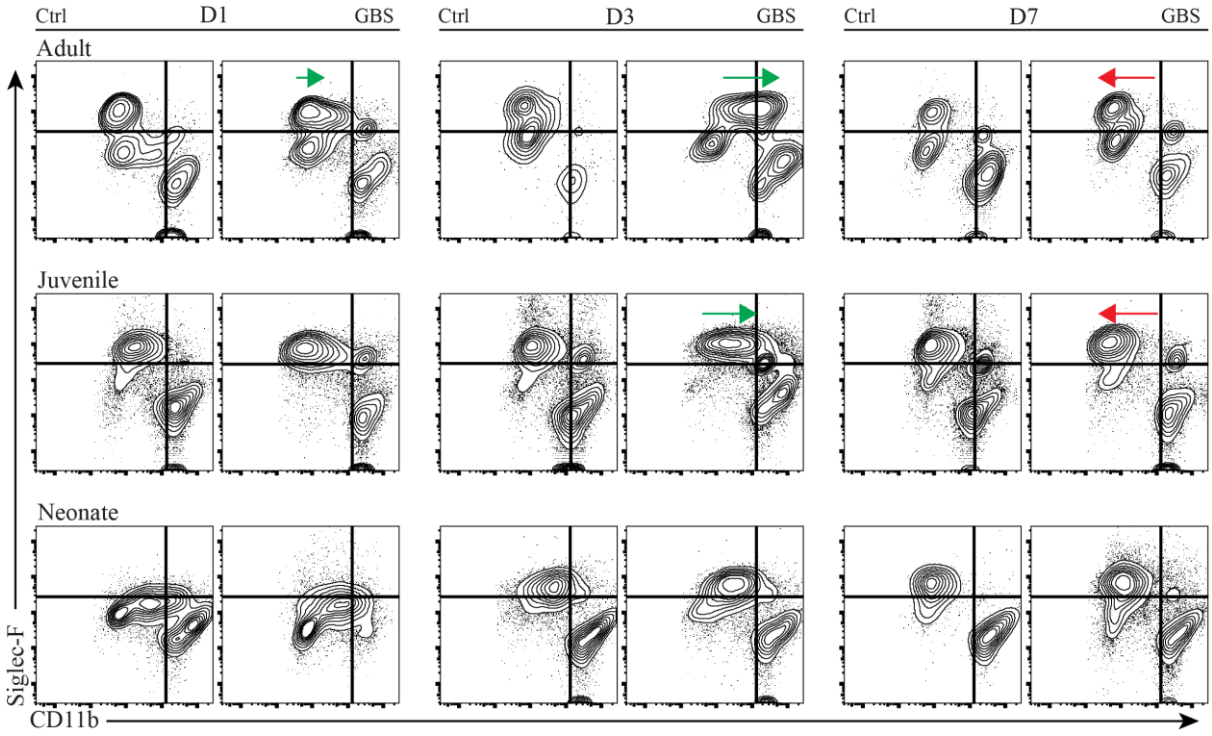

Figure S2 (Refers to Figure 3). Changes in Macrophage Marker Expression Following GBS Infection.

Figure S3 (Refers to Figures 3, 4). Effects of Clodronate on Sn Expression and Backgating Analysis.
(A) Backgating analysis of Sialoadhesin expressing cells seen in adult and juvenile mice and extrapolated to neonates. Sialoadhesin expression restricted to AMϕ populations in adult and juvenile mice and pre-alveolar macrophages in neonates.
(B) Backgating analysis of Siglec-E expression shows both alveolar and interstitial lung macrophage populations express Siglec-E.
(C) Intranasal liposomal clodronate depleted the adult lung of Sialoadhesin-expressing macrophages consistent with restriction to AMϕ populations. Control animals were given empty liposomes for comparison. Error bars represent SEM * $P < 0.05$, $n = 4$.

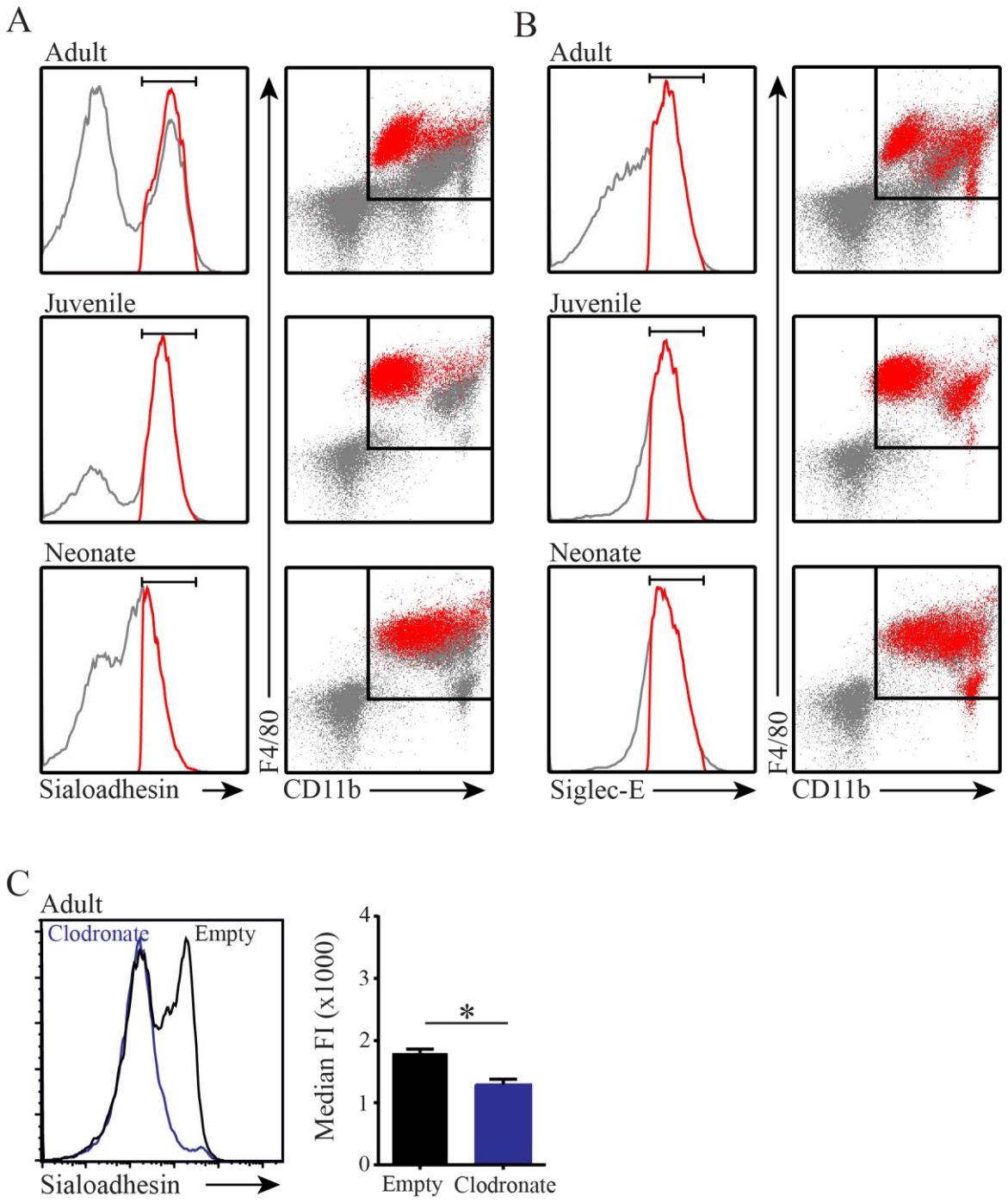

Figure S3 (Refers to Figures 3, 4). Effects of Clodronate on Sn Expression and Backgating Analysis.

Table 1. qPCR Primers

Gene	Forward Primer (5’ – 3’)	Reverse Primer (5’ – 3’)
Gapdh	AGTATGACTCCACTCACGGC	CACCAGTAGACTCCACGACA
Il1b	GGAGAACCAAGCAACGACAAAATA	TGGGGAACTCTGCAGACTCAAAC
Il6	AAACCGCTATGAAGTTCCTCTCTG	ATCCTCTGTGAAGTCTCCTCTCC
Cxcl1	CAGCCACCCGCTCGCTTCTC	TCAAGGCAAGCCTCGCGACCAT
Siglec1	GCTGGTGGACAAGCGTTTC	TTCAAGTCTTTGAGCAACAGGT
Siglece	GTCTCCACAGAGCAGTGCAACTTTATC	TGGGATTCAACCAGGGGATTCTGAG

Table 2. Immune Cell Population Definitions

Cell Population	Surface Marker Definition
AMϕ	$CD45^{+}$ $F4/80^{hi}$ $CD11b^{lo}$ $CD11c^{+}$ $Siglec\text{-}F^{+}$
$CD11b^{+}$ AMϕ	$CD45^{+}$ $F4/80^{hi}$ $CD11b^{hi}$ $CD11c^{+}$ $Siglec\text{-}F^{+}$
NAMϕ	$CD45^{+}$ $F4/80^{hi}$ $CD11b^{lo}$ $CD11c^{lo}$ $Siglec\text{-}F^{lo}$
$CD11c^{-}$ IMϕ	$CD45^{+}$ $F4/80^{lo}$ $CD11b^{hi}$ $CD11c^{-}$ $Siglec\text{-}F^{-}$
$CD11c^{+}$ IMϕ/DC	$CD45^{+}$ $F4/80^{lo}$ $CD11b^{hi}$ $CD11c^{+}$ $Siglec\text{-}F^{-}$
PMN	$CD45^{+}$ $F4/80^{-}$ $CD11b^{hi}$ $CD64^{-}$

This dissertation contains material as it appears in "Developmental Immaturity of Siglec Receptor Expression on Neonatal Alveolar Macrophages Predisposes to Severe Group B Streptococcal Infection" published in *iScience*. The dissertation author was the primary investigator and author of this paper,

> Lund, S. J., Patras, K.A., Kimmey, J.M., Yamamura, A., Butcher, L.D., Del Rosario, P.G.B., Hernandez, G.E., McCoy, A.M., Lakhdari, O., Nizet, V., Prince, L.S. (2020). Developmental Immaturity of Siglec Receptor Expression on Neonatal Alveolar Macrophages Predisposes to Severe Group B Streptococcal Infection. *iScience*, p.101207.

Other material in this dissertation has been adapted from the below manuscript currently in preparation for submission.

> Lund, S. J., Del Rosario, P.G.B., Yamamura, A., Patras, K.A., Butcher, L.D., Lakhdari, O., Nizet, V., Prince, L.S. Sialic Acid-Siglec-E Interactions Regulate Expression of Sialoadhesin and Alveolar Macrophage Development.

REFERENCES

1. Russell, N. J., A. C. Seale, C. O'Sullivan, K. Le Doare, P. T. Heath, J. E. Lawn, L. Bartlett, C. Cutland, M. Gravett, M. Ip, S. A. Madhi, C. E. Rubens, S. K. Saha, S. Schrag, A. Sobanjo-ter Meulen, J. Vekemans, and C. J. Baker. 2017. Risk of Early-Onset Neonatal Group B Streptococcal Disease With Maternal Colonization Worldwide: Systematic Review and Meta-analyses. *Clinical Infectious Diseases* 65: S152-S159.

2. Madrid, L., A. C. Seale, M. Kohli-Lynch, K. M. Edmond, J. E. Lawn, P. T. Heath, S. A. Madhi, C. J. Baker, L. Bartlett, C. Cutland, M. G. Gravett, M. Ip, K. Le Doare, C. E. Rubens, S. K. Saha, A. Sobanjo-ter Meulen, J. Vekemans, S. Schrag, and f. t. I. G. D. I. Group. 2017. Infant Group B Streptococcal Disease Incidence and Serotypes Worldwide: Systematic Review and Meta-analyses. *Clinical Infectious Diseases* 65: S160-S172.

3. Seale, A. C., F. Bianchi-Jassir, N. J. Russell, M. Kohli-Lynch, C. J. Tann, J. Hall, L. Madrid, H. Blencowe, S. Cousens, C. J. Baker, L. Bartlett, C. Cutland, M. G. Gravett, P. T. Heath, M. Ip, K. Le Doare, S. A. Madhi, C. E. Rubens, S. K. Saha, S. J. Schrag, A. Sobanjo-ter Meulen, J. Vekemans, and J. E. Lawn. 2017. Estimates of the Burden of Group B Streptococcal Disease Worldwide for Pregnant Women, Stillbirths, and Children. *Clinical Infectious Diseases* 65: S200-S219.

4. Baker, C. J., and F. F. Barrett. 1973. Transmission of group B streptococci among parturient women and their neonates. *J Pediatr* 83: 919-925.

5. Franciosi, R. A., J. D. Knostman, and R. A. Zimmerman. 1973. Group B streptococcal neonatal and infant infections. *J Pediatr* 82: 707-718.

6. Horn, K. A., W. T. Meyer, B. C. Wyrick, and R. A. Zimmerman. 1974. Group B Streptococcal Neonatal Infection. *JAMA* 230: 1165-1167.

7. Randis, T. M., J. A. Baker, and A. J. Ratner. 2017. Group B Streptococcal Infections. *Pediatrics in Review* 38: 254-262.

8. Raabe, V. N., and A. L. Shane. 2019. Group B Streptococcus (Streptococcus agalactiae). *Microbiology Spectrum* 7.

9. Pitts, S. I., N. M. Maruthur, G. E. Langley, T. Pondo, K. A. Shutt, R. Hollick, S. J. Schrag, A. Thomas, M. Nichols, M. Farley, J. P. Watt, L. Miller, W. Schaffner, C. Holtzman, and L. H. Harrison. 2018. Obesity, Diabetes, and the Risk of Invasive Group B Streptococcal Disease in Nonpregnant Adults in the United States. *Open Forum Infectious Diseases* 5.

10. Skoff, T. H., M. M. Farley, S. Petit, A. S. Craig, W. Schaffner, K. Gershman, L. H. Harrison, R. Lynfield, J. Mohle-Boetani, S. Zansky, B. A. Albanese, K. Stefonek, E.

R. Zell, D. Jackson, T. Thompson, and S. J. Schrag. 2009. Increasing burden of invasive group B streptococcal disease in nonpregnant adults, 1990-2007. *Clin Infect Dis* 49: 85-92.

11. Doran, K. S., J. C. Chang, V. M. Benoit, L. Eckmann, and V. Nizet. 2002. Group B streptococcal beta-hemolysin/cytolysin promotes invasion of human lung epithelial cells and the release of interleukin-8. *J Infect Dis* 185: 196-203.

12. Hensler, M. E., G. Y. Liu, S. Sobczak, K. Benirschke, V. Nizet, and G. P. Heldt. 2005. Virulence role of group B Streptococcus beta-hemolysin/cytolysin in a neonatal rabbit model of early-onset pulmonary infection. *The Journal of infectious diseases* 191: 1287-1291.

13. Herting, E., O. Gefeller, M. Land, L. van Sonderen, K. Harms, and B. Robertson. 2000. Surfactant treatment of neonates with respiratory failure and group B streptococcal infection. Members of the Collaborative European Multicenter Study Group. *Pediatrics* 106: 957-964; discussion 1135.

14. Wessels, M. R. 1997. Biology of streptococcal capsular polysaccharides. *Journal of applied microbiology* 83: 20s-31s.

15. Jennings, H. J., K. G. Rosell, and D. L. Kasper. 1980. Structural determination and serology of the native polysaccharide antigen of type-III group B Streptococcus. *Canadian journal of biochemistry* 58: 112-120.

16. Lewis, A. L., V. Nizet, and A. Varki. 2004. Discovery and characterization of sialic acid O-acetylation in group B Streptococcus. *Proc Natl Acad Sci U S A* 101: 11123-11128.

17. Nicholls, J. M., A. J. Bourne, H. Chen, Y. Guan, and J. S. M. Peiris. 2007. Sialic acid receptor detection in the human respiratory tract: evidence for widespread distribution of potential binding sites for human and avian influenza viruses. *Respiratory Research* 8: 73.

18. Courtney, A. H., E. B. Puffer, J. K. Pontrello, Z. Q. Yang, and L. L. Kiessling. 2009. Sialylated multivalent antigens engage CD22 in trans and inhibit B cell activation. *Proc Natl Acad Sci U S A* 106: 2500-2505.

19. Lübbers, J., E. Rodríguez, and Y. van Kooyk. 2018. Modulation of Immune Tolerance via Siglec-Sialic Acid Interactions. *Frontiers in immunology* 9: 2807-2807.

20. Sjoberg, E. R., L. D. Powell, A. Klein, and A. Varki. 1994. Natural ligands of the B cell adhesion molecule CD22 beta can be masked by 9-O-acetylation of sialic acids. *J Cell Biol* 126: 549-562.

21. Chang, Y.-C., J. Olson, F. C. Beasley, C. Tung, J. Zhang, P. R. Crocker, A. Varki, and V. Nizet. 2014. Group B Streptococcus Engages an Inhibitory Siglec through Sialic Acid Mimicry to Blunt Innate Immune and Inflammatory Responses In Vivo. *PLOS Pathogens* 10: e1003846.

22. Crocker, P. R., J. C. Paulson, and A. Varki. 2007. Siglecs and their roles in the immune system. *Nat Rev Immunol* 7: 255-266.

23. Wessels, M., V. Benedi, D. Kasper, L. Heggen, and C. Rubens. 1991. Type III capsule and virulence of group B streptococci. *Genetics and molecular biology of streptococci, lactococci, and enterococci. American Society for Microbiology, Washington, DC*: 219-223.

24. Marques, M. B., D. L. Kasper, M. K. Pangburn, and M. R. Wessels. 1992. Prevention of C3 deposition by capsular polysaccharide is a virulence mechanism of type III group B streptococci. *Infection and Immunity* 60: 3986-3993.

25. Schittny, J. C. 2017. Development of the lung. *Cell and tissue research* 367: 427-444.

26. Morrisey, E. E., and B. L. M. Hogan. 2010. Preparing for the First Breath: Genetic and Cellular Mechanisms in Lung Development. *Developmental Cell* 18: 8-23.

27. Perdiguero, E. G., and F. Geissmann. 2016. The development and maintenance of resident macrophages. *Nat Immunol* 17: 2-8.

28. Ginhoux, F., and M. Guilliams. 2016. Tissue-Resident Macrophage Ontogeny and Homeostasis. *Immunity* 44: 439-449.

29. Ginhoux, F., M. Greter, M. Leboeuf, S. Nandi, P. See, S. Gokhan, M. F. Mehler, S. J. Conway, L. G. Ng, E. R. Stanley, I. M. Samokhvalov, and M. Merad. 2010. Fate Mapping Analysis Reveals That Adult Microglia Derive from Primitive Macrophages. *Science* 330: 841-845.

30. Tan, S. Y. S., and M. A. Krasnow. 2016. Developmental origin of lung macrophage diversity. *Development* 143: 1318-1327.

31. Kopf, M., C. Schneider, and S. P. Nobs. 2015. The development and function of lung-resident macrophages and dendritic cells. *Nature immunology* 16: 36.

32. Naito, M., K. Takahashi, and S. Nishikawa. 1990. Development, differentiation, and maturation of macrophages in the fetal mouse liver. *Journal of leukocyte biology* 48: 27-37.

33. Guilliams, M., I. De Kleer, S. Henri, S. Post, L. Vanhoutte, S. De Prijck, K. Deswarte, B. Malissen, H. Hammad, and B. N. Lambrecht. 2013. Alveolar macrophages develop

from fetal monocytes that differentiate into long-lived cells in the first week of life via GM-CSF. *The Journal of Experimental Medicine*.

34. Schneider, C., S. P. Nobs, M. Kurrer, H. Rehrauer, C. Thiele, and M. Kopf. 2014. Induction of the nuclear receptor PPAR-gamma by the cytokine GM-CSF is critical for the differentiation of fetal monocytes into alveolar macrophages. *Nat Immunol* 15: 1026-1037.

35. Lakhdari, O., A. Yamamura, G. E. Hernandez, K. K. Anderson, S. J. Lund, G. O. Oppong-Nonterah, H. M. Hoffman, and L. S. Prince. 2019. Differential Immune Activation in Fetal Macrophage Populations. *Sci Rep* 9: 7677.

36. van de Laar, L., W. Saelens, S. De Prijck, L. Martens, C. L. Scott, G. Van Isterdael, E. Hoffmann, R. Beyaert, Y. Saeys, B. N. Lambrecht, and M. Guilliams. 2016. Yolk Sac Macrophages, Fetal Liver, and Adult Monocytes Can Colonize an Empty Niche and Develop into Functional Tissue-Resident Macrophages. *Immunity* 44: 755-768.

37. Allard, B., A. Panariti, and J. G. Martin. 2018. Alveolar macrophages in the resolution of inflammation, tissue repair, and tolerance to infection. *Frontiers in immunology* 9.

38. Byrne, A. J., S. A. Mathie, L. G. Gregory, and C. M. Lloyd. 2015. Pulmonary macrophages: key players in the innate defence of the airways. *Thorax* 70: 1189-1196.

39. Kopf, M., C. Schneider, and S. P. Nobs. 2015. The development and function of lung-resident macrophages and dendritic cells. *Nat Immunol* 16: 36-44.

40. Todd, E. M., J. Y. Zhou, T. P. Szasz, L. E. Deady, J. A. D'Angelo, M. D. Cheung, A. H. Kim, and S. C. Morley. 2016. Alveolar macrophage development in mice requires L-plastin for cellular localization in alveoli. *Blood* 128: 2785-2796.

41. Guilliams, M., I. De Kleer, S. Henri, S. Post, L. Vanhoutte, S. De Prijck, K. Deswarte, B. Malissen, H. Hammad, and B. N. Lambrecht. 2013. Alveolar macrophages develop from fetal monocytes that differentiate into long-lived cells in the first week of life via GM-CSF. *The Journal of experimental medicine* 210: 1977-1992.

42. Berclaz, P.-Y., Y. Shibata, J. A. Whitsett, and B. C. Trapnell. 2002. GM-CSF, via PU.1, regulates alveolar macrophage FcγR-mediated phagocytosis and the IL-18/IFN-γ–mediated molecular connection between innate and adaptive immunity in the lung. *Blood* 100: 4193-4200.

43. Shibata, Y., P.-Y. Berclaz, Z. C. Chroneos, M. Yoshida, J. A. Whitsett, and B. C. Trapnell. 2001. GM-CSF Regulates Alveolar Macrophage Differentiation and Innate Immunity in the Lung through PU.1. *Immunity* 15: 557-567.

44. Yu, X., A. Buttgereit, I. Lelios, S. G. Utz, D. Cansever, B. Becher, and M. Greter. 2017. The Cytokine TGF-beta Promotes the Development and Homeostasis of Alveolar Macrophages. *Immunity* 47: 903-912.e904.

45. Bonfield, T. L., C. F. Farver, B. P. Barna, A. Malur, S. Abraham, B. Raychaudhuri, M. S. Kavuru, and M. J. Thomassen. 2003. Peroxisome Proliferator-Activated Receptor-γ Is Deficient in Alveolar Macrophages from Patients with Alveolar Proteinosis. *American Journal of Respiratory Cell and Molecular Biology* 29: 677-682.

46. Bonfield, T. L., M. J. Thomassen, C. F. Farver, S. Abraham, M. T. Koloze, X. Zhang, D. M. Mosser, and D. A. Culver. 2008. Peroxisome Proliferator-Activated Receptor-γ Regulates the Expression of Alveolar Macrophage Macrophage Colony-Stimulating Factor. *The Journal of Immunology* 181: 235-242.

47. Cai, Y., C. Sugimoto, M. Arainga, X. Alvarez, E. S. Didier, and M. J. Kuroda. 2014. In vivo characterization of alveolar and interstitial lung macrophages in rhesus macaques: implications for understanding lung disease in humans. *J Immunol* 192: 2821-2829.

48. Gibbings, S. L., S. M. Thomas, S. M. Atif, A. L. McCubbrey, A. N. Desch, T. Danhorn, S. M. Leach, D. L. Bratton, P. M. Henson, W. J. Janssen, and C. V. Jakubzick. 2017. Three Unique Interstitial Macrophages in the Murine Lung at Steady State. *Am J Respir Cell Mol Biol* 57: 66-76.

49. Ural, B. B., S. T. Yeung, P. Damani-Yokota, J. C. Devlin, M. de Vries, P. Vera-Licona, T. Samji, C. M. Sawai, G. Jang, O. A. Perez, Q. Pham, L. Maher, P. n. Loke, M. Dittmann, B. Reizis, and K. M. Khanna. 2020. Identification of a nerve-associated, lung-resident interstitial macrophage subset with distinct localization and immunoregulatory properties. *Science Immunology* 5: eaax8756.

50. Weitnauer, M., V. Mijosek, and A. H. Dalpke. 2016. Control of local immunity by airway epithelial cells. *Mucosal Immunol* 9: 287-298.

51. Whitsett, J. A., and T. Alenghat. 2015. Respiratory epithelial cells orchestrate pulmonary innate immunity. *Nat Immunol* 16: 27-35.

52. Fliegauf, M., A. F. P. Sonnen, B. Kremer, and P. Henneke. 2013. Mucociliary clearance defects in a murine in vitro model of pneumococcal airway infection. *PloS one* 8: e59925-e59925.

53. LeVine, A. M., J. A. Reed, K. E. Kurak, E. Cianciolo, and J. A. Whitsett. 1999. GM-CSF–deficient mice are susceptible to pulmonary group B streptococcal infection. *The Journal of Clinical Investigation* 103: 563-569.

54. Biondo, C., G. Mancuso, A. Midiri, G. Signorino, M. Domina, V. Lanza Cariccio, M. Venza, I. Venza, G. Teti, and C. Beninati. 2014. Essential role of interleukin-1 signaling in host defenses against group B streptococcus. *MBio* 5: e01428-01414.

55. Costa, A., R. Gupta, G. Signorino, A. Malara, F. Cardile, C. Biondo, A. Midiri, R. Galbo, P. Trieu-Cuot, S. Papasergi, G. Teti, P. Henneke, G. Mancuso, D. T. Golenbock, and C. Beninati. 2012. Activation of the NLRP3 inflammasome by group B streptococci. *Journal of immunology (Baltimore, Md. : 1950)* 188: 1953-1960.

56. Chang, Y. C., J. Olson, A. Louie, P. R. Crocker, A. Varki, and V. Nizet. 2014. Role of macrophage sialoadhesin in host defense against the sialylated pathogen group B Streptococcus. *J Mol Med (Berl)* 92: 951-959.

57. Oetke, C., M. C. Vinson, C. Jones, and P. R. Crocker. 2006. Sialoadhesin-Deficient Mice Exhibit Subtle Changes in B- and T-Cell Populations and Reduced Immunoglobulin M Levels. *Molecular and Cellular Biology* 26: 1549-1557.

58. Andrade, E. B., A. Magalhaes, A. Puga, M. Costa, J. Bravo, C. C. Portugal, A. Ribeiro, M. Correia-Neves, A. Faustino, A. Firon, P. Trieu-Cuot, T. Summavielle, and P. Ferreira. 2018. A mouse model reproducing the pathophysiology of neonatal group B streptococcal infection. *Nature communications* 9: 3138.

59. Doran, K. S., G. Y. Liu, and V. Nizet. 2003. Group B streptococcal β-hemolysin/cytolysin activates neutrophil signaling pathways in brain endothelium and contributes to development of meningitis. *The Journal of clinical investigation* 112: 736-744.

60. Hensler, M. E., D. Quach, C.-J. Hsieh, K. S. Doran, and V. Nizet. 2008. CAMP factor is not essential for systemic virulence of Group B Streptococcus. *Microbial pathogenesis* 44: 84-88.

61. Yim, H. H., A. Nittayarin, and C. E. Rubens. 1997. Analysis of the Capsule Synthesis Locus, A Virulence Factor in Group B Streptococci. In *Streptococci and the Host*. T. Horaud, A. Bouvet, R. Leclercq, H. de Montclos, and M. Sicard, eds. Springer US, Boston, MA. 995-997.

62. Sakai, M., T. D. Troutman, J. S. Seidman, Z. Ouyang, N. J. Spann, Y. Abe, K. M. Ego, C. M. Bruni, Z. Deng, J. C. M. Schlachetzki, A. Nott, H. Bennett, J. Chang, B. T. Vu, M. P. Pasillas, V. M. Link, L. Texari, S. Heinz, B. M. Thompson, J. G. McDonald, F. Geissmann, and C. K. Glass. 2019. Liver-Derived Signals Sequentially Reprogram Myeloid Enhancers to Initiate and Maintain Kupffer Cell Identity. *Immunity* 51: 655-670.e658.

63. Duan, M., W. C. Li, R. Vlahos, M. J. Maxwell, G. P. Anderson, and M. L. Hibbs. 2012. Distinct macrophage subpopulations characterize acute infection and chronic inflammatory lung disease. *J Immunol* 189: 946-955.

64. Duan, M., D. P. Steinfort, D. Smallwood, M. Hew, W. Chen, M. Ernst, L. B. Irving, G. P. Anderson, and M. L. Hibbs. 2016. CD11b immunophenotyping identifies inflammatory profiles in the mouse and human lungs. *Mucosal Immunol* 9: 550-563.

65. Zhou, K.-R., S. Liu, W.-J. Sun, L.-L. Zheng, H. Zhou, J.-H. Yang, and L.-H. Qu. 2017. ChIPBase v2.0: decoding transcriptional regulatory networks of non-coding RNAs and protein-coding genes from ChIP-seq data. *Nucleic Acids Res* 45: D43-D50.

66. Kreft, L., A. Soete, P. Hulpiau, A. Botzki, Y. Saeys, and P. De Bleser. 2017. ConTra v3: a tool to identify transcription factor binding sites across species, update 2017. *Nucleic Acids Res* 45: W490-W494.

67. Van Bockstal, L., D. Bulté, M. Van den Kerkhof, L. Dirkx, D. Mabille, S. Hendrickx, P. Delputte, L. Maes, and G. Caljon. 2020. Interferon Alpha Favors Macrophage Infection by Visceral Leishmania Species Through Upregulation of Sialoadhesin Expression. *Frontiers in Immunology* 11.

68. Rempel, H., C. Calosing, B. Sun, and L. Pulliam. 2008. Sialoadhesin Expressed on IFN-Induced Monocytes Binds HIV-1 and Enhances Infectivity. *PLOS ONE* 3: e1967.

69. Fercoq, F., E. Remion, S. J. Frohberger, N. Vallarino-Lhermitte, A. Hoerauf, J. Le Quesne, F. Landmann, M. P. Hübner, L. M. Carlin, and C. Martin. 2019. IL-4 receptor dependent expansion of lung CD169+ macrophages in microfilaria-driven inflammation. *PLoS neglected tropical diseases* 13: e0007691.

70. Toshchakov, V., B. W. Jones, A. Lentschat, A. Silva, P. Y. Perera, K. Thomas, M. J. Cody, S. Zhang, B. R. Williams, J. Major, T. A. Hamilton, M. J. Fenton, and S. N. Vogel. 2003. TLR2 and TLR4 agonists stimulate unique repertoires of host resistance genes in murine macrophages: interferon-beta-dependent signaling in TLR4-mediated responses. *Journal of endotoxin research* 9: 169-175.

71. Toshchakov, V., B. W. Jones, P. Y. Perera, K. Thomas, M. J. Cody, S. Zhang, B. R. Williams, J. Major, T. A. Hamilton, M. J. Fenton, and S. N. Vogel. 2002. TLR4, but not TLR2, mediates IFN-beta-induced STAT1alpha/beta-dependent gene expression in macrophages. *Nat Immunol* 3: 392-398.

72. Faraggiana, T., D. Villari, J. Jagirdar, and J. Patil. 1986. Expression of sialic acid on the alveolar surface of adult and fetal human lungs. *The journal of histochemistry and cytochemistry : official journal of the Histochemistry Society* 34: 811-816.

73. Ibricevic, A., A. Pekosz, M. J. Walter, C. Newby, J. T. Battaile, E. G. Brown, M. J. Holtzman, and S. L. Brody. 2006. Influenza virus receptor specificity and cell tropism in mouse and human airway epithelial cells. *J Virol* 80: 7469-7480.

74. Patras, K. A., A. Coady, J. Olson, S. R. Ali, S. P. RamachandraRao, S. Kumar, A. Varki, and V. Nizet. 2017. Tamm–Horsfall glycoprotein engages human Siglec-9 to modulate neutrophil activation in the urinary tract. *Immunology & Cell Biology* 95: 960-965.

75. Bebien, M., M. E. Hensler, S. Davanture, L.-C. Hsu, M. Karin, J. M. Park, L. Alexopoulou, G. Y. Liu, V. Nizet, and T. Lawrence. 2012. The pore-forming toxin β hemolysin/cytolysin triggers p38 MAPK-dependent IL-10 production in macrophages and inhibits innate immunity. *PLoS Pathog* 8: e1002812.

76. Evans, S. E., Y. Xu, M. J. Tuvim, and B. F. Dickey. 2010. Inducible innate resistance of lung epithelium to infection. *Annu Rev Physiol* 72: 413-435.

77. Lambert, L., and F. J. Culley. 2017. Innate Immunity to Respiratory Infection in Early Life. *Frontiers in Immunology* 8.

78. Nicod, L. P. 2005. Lung defences: an overview. *European Respiratory Review* 14: 45-50.

79. Micanovic, R., K. LaFavers, P. S. Garimella, X. R. Wu, and T. M. El-Achkar. 2020. Uromodulin (Tamm-Horsfall protein): guardian of urinary and systemic homeostasis. *Nephrology, dialysis, transplantation : official publication of the European Dialysis and Transplant Association - European Renal Association* 35: 33-43.

80. Micanovic, R., B. R. Chitteti, P. C. Dagher, E. F. Srour, S. Khan, T. Hato, A. Lyle, Y. Tong, X. R. Wu, and T. M. El-Achkar. 2015. Tamm-Horsfall Protein Regulates Granulopoiesis and Systemic Neutrophil Homeostasis. *Journal of the American Society of Nephrology : JASN* 26: 2172-2182.

81. Muchmore, A. V., and J. M. Decker. 1987. Evidence that recombinant IL 1 alpha exhibits lectin-like specificity and binds to homogeneous uromodulin via N-linked oligosaccharides. *J Immunol* 138: 2541-2546.

82. Sherblom, A. P., J. M. Decker, and A. V. Muchmore. 1988. The lectin-like interaction between recombinant tumor necrosis factor and uromodulin. *J Biol Chem* 263: 5418-5424.

83. Rhodes, D. C. 2002. Binding of Tamm-Horsfall protein to complement 1q and complement 1, including influence of hydrogen-ion concentration. *Immunol Cell Biol* 80: 558-566.

84. Sherblom, A. P., N. Sathyamoorthy, J. M. Decker, and A. V. Muchmore. 1989. IL-2, a lectin with specificity for high mannose glycopeptides. *J Immunol* 143: 939-944.

85. Stouch, A. N., A. M. McCoy, R. M. Greer, O. Lakhdari, F. E. Yull, T. S. Blackwell, H. M. Hoffman, and L. S. Prince. 2016. IL-1beta and Inflammasome Activity Link Inflammation to Abnormal Fetal Airway Development. *J Immunol* 196: 3411-3420.